Electrochemistry of Adsorbed Organic Dye Molecules

Thesis by

Deidre A. Askew

In Partial Fulfillment of the Requirements

for the Degree of

Master of Science

California Institute of Technology

Pasadena, California

Submitted May 25, 1984

ABSTRACT

Molecular luminescence has been used to study the mechanism of charge transfer in electrode-bound films and coatings. This sensitive, fast technique enables one to observe occurrences on the electrode surface which could not be observed with conventional electrochemical or spectroelectrochemical methods. In general, electrodes should be excellent quenchers of fluorescence due to energy transfer or electron transfer. We want to examine the mechanism of the surface quenching of the fluorescence. By reproducibly adsorbing a known amount of an organic dye of high quantum yield to the electrode surface, one should be able to determine if electron transfer is a pathway in the quenching mechanism by varying the potential of the electrode. This report describes the electrochemistry of several organic dyes adsorbed on graphite electrodes which could be used for the luminescence studies. Methylene blue adsorption and electrochemistry are studied in detail. The methylene blue system is excellent in terms of adsorption characteristics. Adsorption isotherms are presented which show the range of surface coverage, Γ, that one can achieve. Methylene blue also has clean reversible electrochemistry to facilitate spectroelectrochemical experiments. However, methylene blue has a small fluorescence quantum yield and short fluorescence lifetime. This may make it a poor choice for luminescence experiments. Several other organic dyes were studied. While their electrochemistry is not as clean as that of methylene blue, their fluorescence quantum yields are much higher.

CONTENTS

1. INTRODUCTION

Molecular luminescence has been used to study the mechanism of charge transfer in electrode-bound films and coatings.[1-7] Fluorescence has been widely used as a probe of structures in biological systems. Although there have been relatively few instances of fluorescence probes near an electrode surface other than semiconductors, the techniques have already been developed to do these experiments. Fluorescence is also a highly sensitive method of detecting surface-bound molecules. Submonolayers have been detected in some experiments.[8] In addition, fluorescence experiments can be conducted on a very short time domain, and the kinetics of fluorescence quenching is well understood. Therefore, it enables one to observe occurrences on the electrode surface which could not be observed with conventional electrochemical or spectroelectrochemical methods.

Faulkner and coworkers were the first to show luminescence from an electroactive species on an electrode surface.[4] This was an unexpected result, since it was predicted that excited molecules at electrodes other than semiconductors would be rapidly quenched, either by energy transfer due to the reversible electron-exchange mechanism or to a Förster type mechanism, or by electron-transfer. In general, electrodes should be excellent quenchers of fluorescence.

We want to examine the mechanism of the surface quenching of the fluorescence. Quenching could be due to energy transfer or electron transfer. Radiationless energy transfer can occur via two types of interactions, the exchange interaction (overlap mechanism) and the coulombic interaction (Förster type energy transfer).[9]

excitation	$D + h\nu \rightarrow D^*$
double electron transfer at electrode	$D^* + e - e \rightarrow D$
Förster energy transfer	$D^* \rightarrow D$
electron transfer	$D^{*x} \pm e \rightarrow D^{x\pm1}$
fluorescence	$D^* \rightarrow D + h\nu$

Figure 1: Excitation of species at electrode surface and possible pathways thereafter.

Consider the following energy transfer situation, in which an excited donor state transfers its energy to an acceptor.

$$D^* + A \rightarrow D + A^*$$

One can view the overlap mechanism simplistically in terms of potential energy surfaces, shown in figure 2. The two species must be in physical contact for their orbitals to overlap sufficiently in space. In the region of overlap, electron exchange may occur. Figure 3 shows the relationship between electron exchange and varying overlap. In general, the rate constant for energy transfer by electron exchange is expected to fall off exponentially as the separation between D^* and A increases. Dexter proposed an expression for the rate constant of energy transfer.[10]

$$k_{ET}(\text{exchange}) = K\,J \exp\left(-\frac{2\,R_{DA}}{L}\right)$$

where

K = constant related to specific orbital interaction;

J = spectral overlap integral normalized for extinction coefficient of

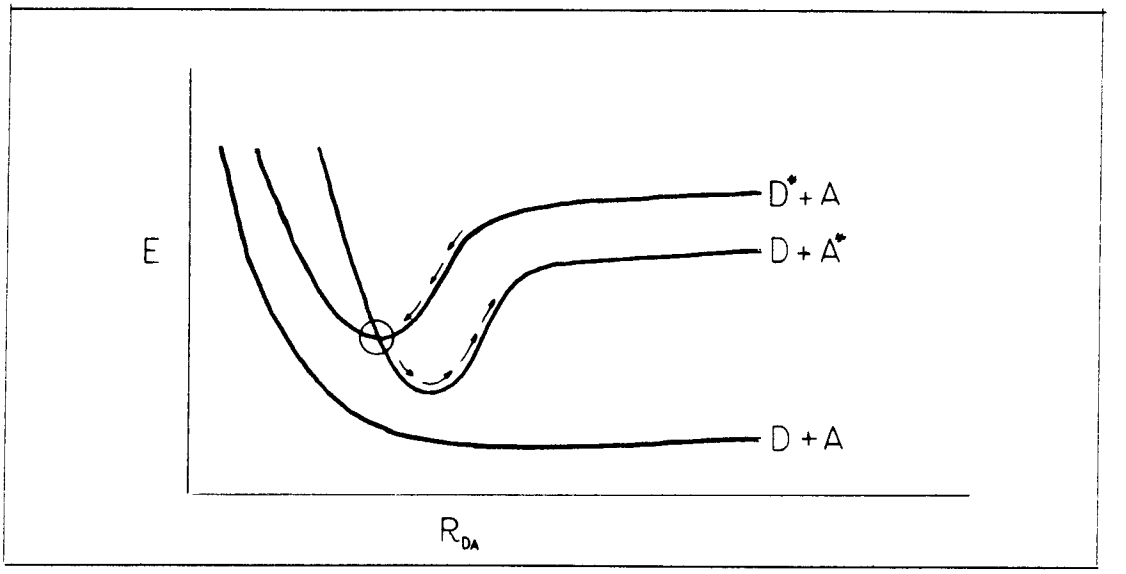

Figure 2: Schematic surface representation of collisional energy transfer (overlap mechanism).

acceptor;

R_{DA} = donor-acceptor separation relative to Van der Waals radii, L.

Since J is normalized for ε_A, it is independent of the acceptor extinction coefficient. Therefore, the exchange rate constant of energy transfer, k_{ET} is predicted to be independent of absorption characteristics of the acceptor, A. The mechanism probably has a greater contribution to the quenching on a surface than it would in a solution, since the surface concentration is very high. The molecules are adsorbed on the surface, and hence, significant overlap of orbitals should occur.

An energy transfer process by the coulombic mechanism does not involve a potential energy surface crossing between the two states, shown in figure 4. In the coulombic interaction, the electric field near an electronically excited molecule is assumed to behave like a field generated by a classical oscillating dipole. This is a result of the motion along the molecular framework of the

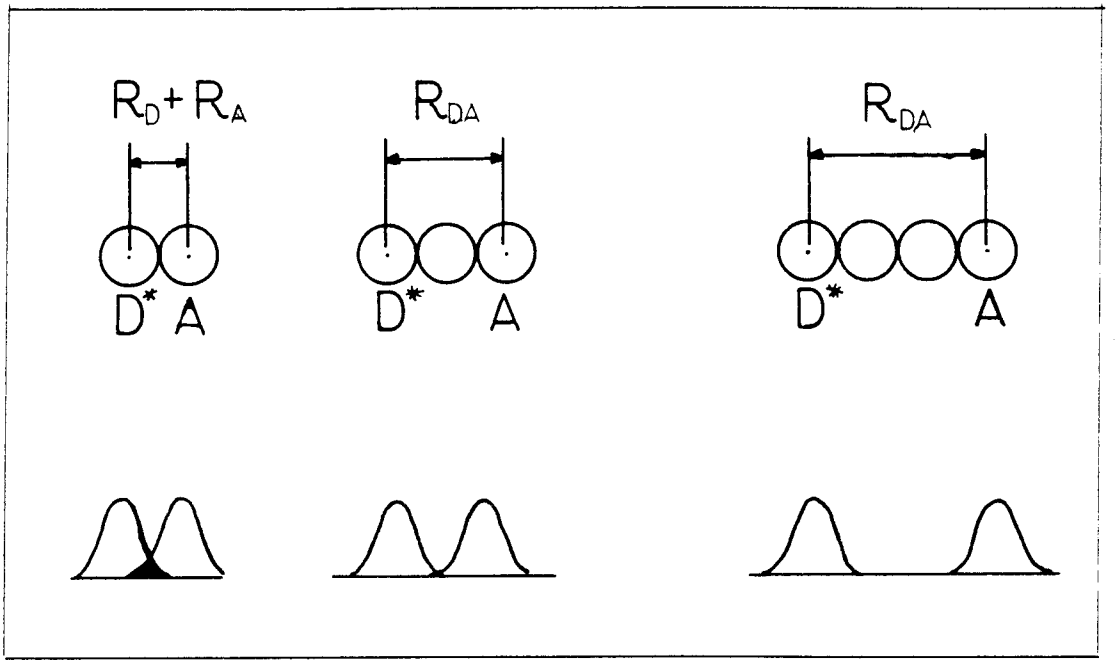

Figure 3: Schematic description of electronic overlap between an electronically excited donor, D^*, and a ground-state acceptor, A, as a function of separation.

excited electron on D^*. This electric charge oscillation causes electrostatic forces to be exerted on the electronic system of nearby molecules. The electrons of a ground state molecule may then begin to oscillate. For A^* to be produced, a resonance condition and a coupling of energy states must occur. The interaction energy, E, between two electric dipoles is related to the magnitude of the two dipoles (μ_D, μ_A) and the distance between them, R_{DA}.[11]

$$E \propto \frac{\mu_D \mu_A}{R_{DA}}$$

Förster related E to experimentally measured oscillator strengths for radiative transitions of D and A. The rate of energy transfer, k_{ET}, by the dipole-dipole mechanism was then related to E^2.[11]

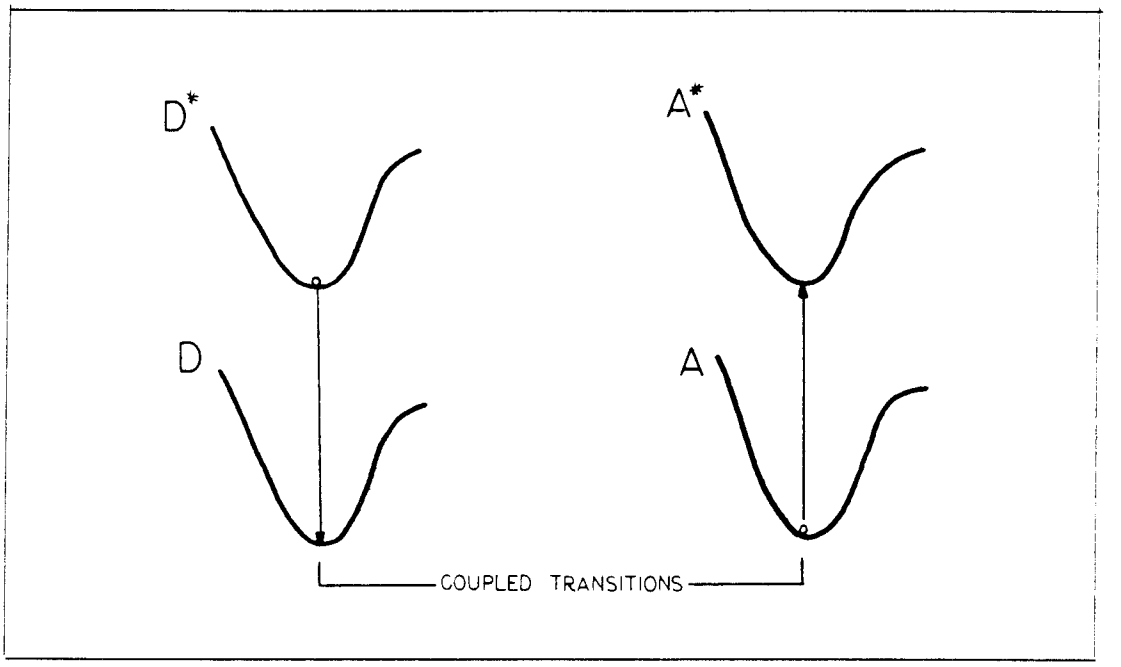

Figure 4: Schematic surface description of energy transfer by the Coulombic mechanism.

$$k_{ET}\,(\text{coulombic}) \rightarrow E^2 \;\alpha\; \left(\frac{\mu_D\,\mu_A}{R^3_{DA}}\right)^2 = \frac{\mu^2_D\,\mu^2_A}{R^6_{DA}}$$

Thus, Förster's theory predicts k_{ET} for energy transfer via this mechanism is proportional to the inverse sixth power of the distance between D^* and A.

A recent publication reported the spectroelectrochemical behavior of ruthenium bis(bipyridyl)4,4'-bis(2-(diphenylamine)ethyl)-2,2'-bipyridine dichloride, $[Ru(bpy)_2(pbby)]Cl_2$ adsorbed on pyrolytic graphite.[12] The purpose of these experiments was to determine the mechanism of surface quenching of the excited state luminescence. The control experiment involved the Ru^{2+} complex evaporated on quartz, which was assumed to be an inert surface on which electron transfer could not occur. The luminescence intensity decay curve obtained was nonexponential, as shown in figure 5. This decay was attributed to

triplet-triplet annihilation (TTA), in which two triplet states undergo energy redistribution to ground state singlet and an excited singlet state, which may undergo a radiationless decay or luminescence, as shown below.

$$D_T + D_T \rightarrow D_{S_1} + D_{S_0}$$

The TTA is due to the relatively high concentration (molar, in some cases) of the species on the surface, but also due to the high intensity of the exciting laser beam. Lowering the laser intensity lessens this effect, but also causes the luminescence intensity to fall below the level of detection. The fluorescence quantum yield of $[Ru(bpy)_2(pbby)]Cl_2$ is only 0.04. In some experiments in which the laser intensity was lowered, the decay curve on quartz did become more nearly exponential.

The same experiment was then done with $[Ru(bpy)_2(pbby)]Cl_2$ adsorbed on edge plane pyrolytic graphite (EPG). As shown in figure 5, the luminescence lifetime was much shorter than that of the complex on quartz. The difference is due mainly to quenching by the electrode surface. The luminescence decay curve could be approximated as the sum of two exponentials, indicating two types of emitting molecules on the surface. The surface quenching could be due to both triplet excitation transfer and electron transfer mechanisms. More experiments, especially with higher luminescence intensities, could allow distinction between the two mechanisms. An extension of this original project, is to find a species with a higher quantum yield to study. This would enable one to lower the laser intensity, eliminating triplet-triplet annihilation, and, also, to study the mechanism of the surface quenching process.

A different mechanism that could contribute to the luminescence quenching is electron transfer. Mataga and Weller have shown that electron transfer

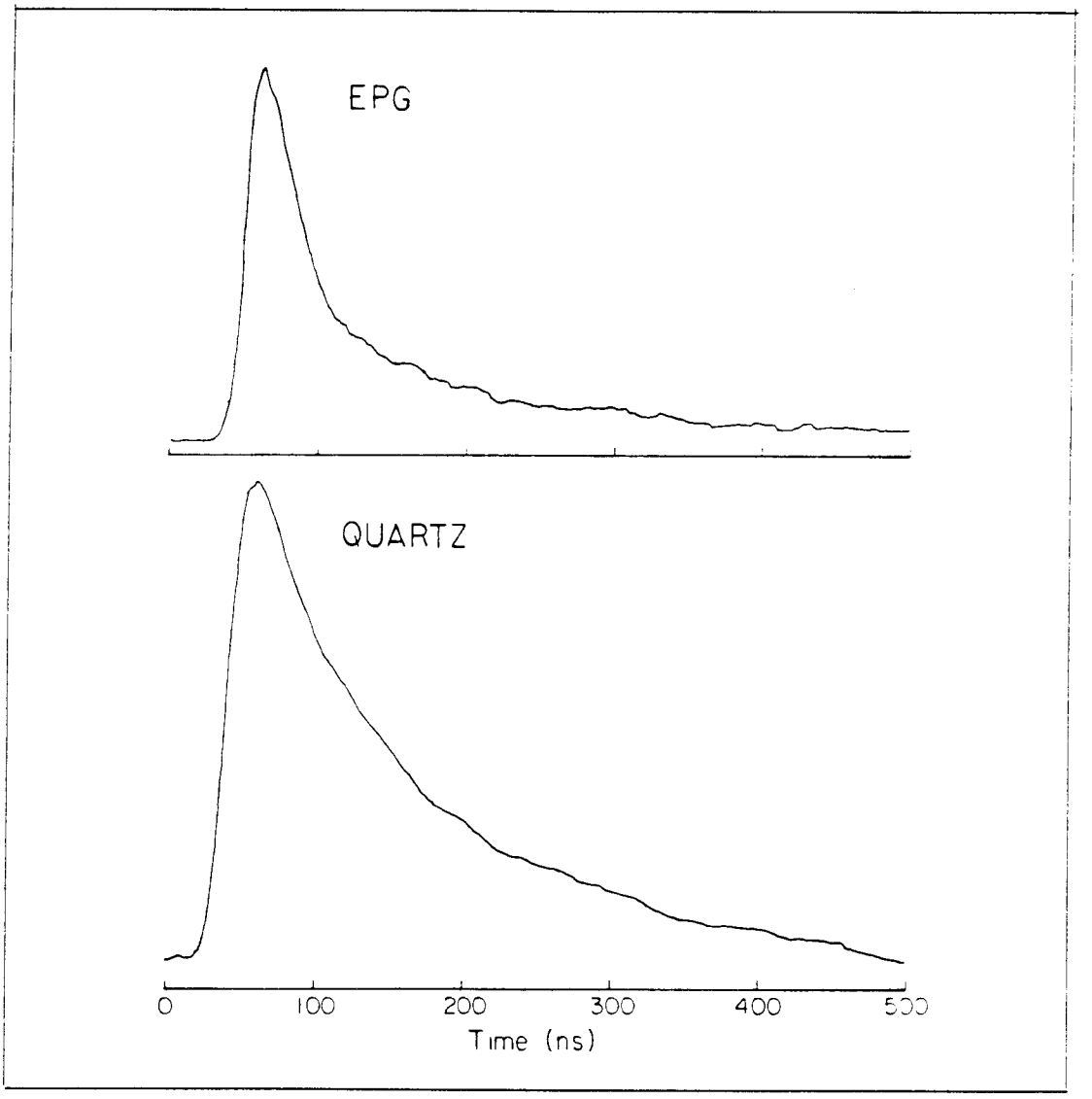

Figure 5: Luminescence decay of $[Ru(bpy)_2(pbpy)]Cl_2$ on quartz and edge plane graphite.[12]

can be a common reaction for organic excited states.[13,14] Metal complex excited states, such as $Ru(bpy)_3^{2+}$, have also shown this reactivity.[15,16] The condition for this to occur is that the molecular excited states are sufficiently long lived to be in thermal equilibrium with their surroundings. This makes them distinct entities having characteristic chemical and physical properties of

their own, including oxidation and reduction potentials. Some redox potentials of excited states have been measured by conducting rate studies for the excited state quenching with quenchers having varying strengths as oxidants. The quenching rate data can be used to estimate excited state redox potentials.[16] We hope to do the same thing by replacing the chemical oxidants with an electrode held at various potentials. At this time, we only wish to establish if electron transfer is a pathway in the surface quenching. One difficulty in our experiment arises from the high concentration of species at the electrode surface. This allows energy transfer among molecules as well as between the species and the electrode. If electron transfer is a pathway, it must occur on a comparative time scale as this intramolecular energy transfer.

A specific problem with organic dyes is their tendency to form dimers, trimers, etc., especially in a region of high concentration such as that on the electrode surface.[17] These larger molecules have increased aromaticity and therefore, lower energy excited states. A relationship is shown in figure 6. Energy transfer will occur until the lowest energy excited state is reached.[18] The larger oligomer dyes do not emit, but instead undergo nonradiative decay.

When luminescence quenching occurs in solid solution, as at the electrode surface, there is no statistical mixing of D^* and A. The Perrin formulation assumes an effective quenching sphere exists around D^*.[19,20] The model is shown in figure 7. The model assumes that the donor and acceptor cannot undergo displacements in space during the D^* lifetime. One can predict a volume in space about D^* whose radius is R, and if a quencher molecule is within this quenching sphere, D^* is deactivated with unit efficiency. If the quencher molecule is outside the quenching sphere, it does not quench D^* at all.

By observing the changes in fluorescence intensity as a function of elec-

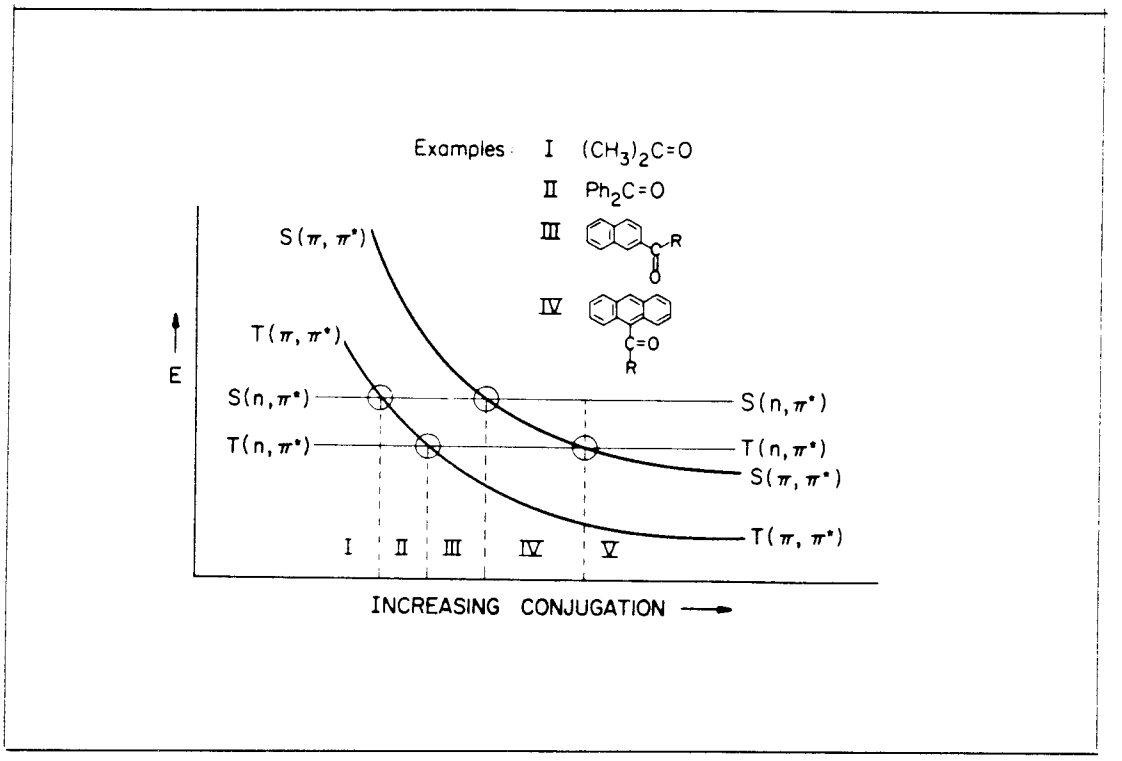

Figure 6: Variation of energy states as a function of increasing conjugation of the system.[9]

trode potential, we hope to determine if the fluorescence quenching occurs via an electron transfer mechanism. An extension of this experiment is to measure the luminescence lifetime of the surface species at different electrode potentials. A change in the lifetimes with varying potentials would indicate an electron transfer mechanism. A potential conducive to oxidation or reduction of the excited state species would result in an electron transfer, and hence, a decrease in the fluorescence lifetime.

Faulkner and coworkers have examined the luminescence of zinc tetraphenylporphyrin (ZnTPP) on pyrolytic graphite while varying the electrode potential.[21] If electron transfer mechanisms are causing the surface quenching, for fluorescence to be observed the electron transfer reaction to and from

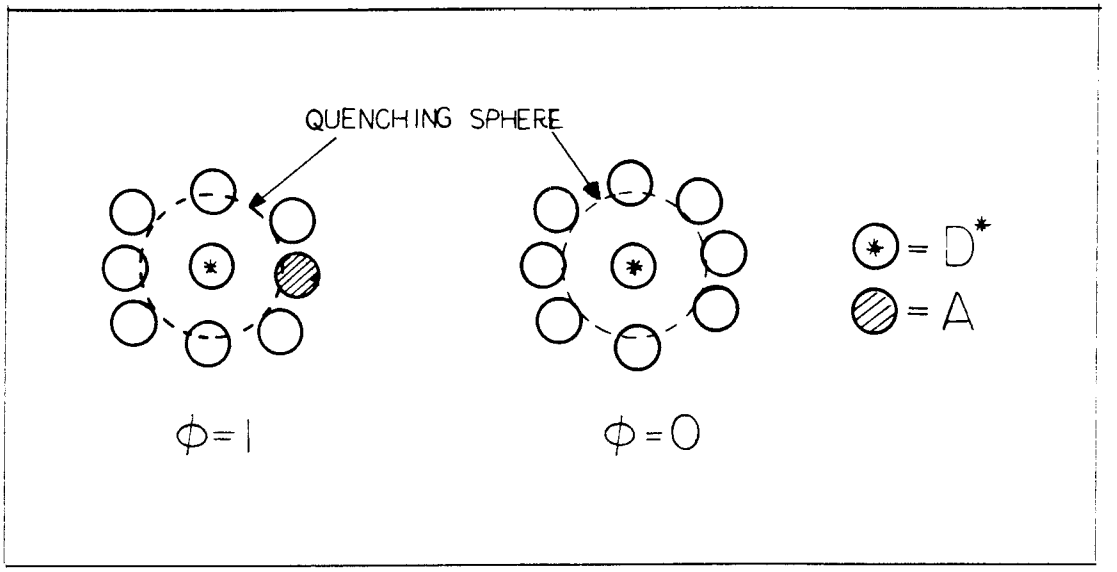

Figure 7: Two-dimensional representation of the Perrin formulation of a quenching sphere about an electronically excited molecule D^*.

the electrode must be sufficiently slow. It is likely, therefore, that fluorescence can only be observed from centers that are not adjacent to the actual electrode surface. Faulkner's simultaneous electrochemical and fluorometric experiments showed that most of the surface species were not able to be directly oxidized. Actually, only 1% of the attached molecules were electroactive. This led to a conclusion that charge propagation by electron exchange did not occur to any great extent. However, the exchange kinetics cannot be that slow, since the oxidation of ZnTPP is reversible on a cyclic voltammetry time scale. Therefore, the electroactive molecules must be at positions conducive to direct electrooxidation, while the other cites must be chemically different, making them electroinactive. However, the oxidized electroactive centers have a large quenching radius. Small degrees of oxidation can produce much larger decreases in relative fluorescence intensity.

Very recently, the fluorescence of an organic dye, Rhodamine B, adsorbed on glass was measured.[8,22] In this system energy transfer and electron transfer could be observed independently. On this surface, the energy transfer was studied, while electron transfer did not occur. The energy transfer occurs from excited dye monomers to non-fluorescing dye aggregates. Therefore, the coverage dependence of the fluorescence and absorption spectra and the fluorescence decay was analyzed. The studies indicated the existence of two types of adsorbed monomers, since the decay could be fit to a two term equation instead of a pure Förster type energy transfer. They considered the phenomenon as two possible configurations, a rigid attachment with a longer lifetime and a more flexible one with a shorter lifetime. These differing lifetimes could be due to enhanced or retarded nonradiative decay channels.

It was important in our project to find a system which the film thickness could be known and varied. This would allow a study of surface quenching effects as the number of adsorbed layers increases. In the $[Ru(bpy)_2(pbpy)]Cl_2$ experiments, this was difficult to do. The solution was pipetted onto the electrode surface, and solvent allowed to evaporate, resulting in irregular surface coverage. An organic dye molecule could be electrochemically loaded, which would ensure a more uniform surface film.

The purpose of this research project was to find suitable organic dye molecules that would adsorb uniformly and reproducibly to the graphite surface. In addition, the dyes were chosen to have high quantum yields. Another characteristic to look for was clean, reversible electrochemistry to facilitate the simultaneous electrochemical/fluorometric experiments.

2. EXPERIMENTAL

2.1 Reagents and Solution Preparation

All solutions are prepared with Barnstead nanopure deionized water. Dyes are obtained from the following sources: methylene blue, MCB Manufacturing Chemists; neutral red, Sigma Chemical Company; Nile blue, National Aniline and Chemical Company, Inc.; acridine orange, Sigma Chemical Company; rhodamine B, Aldrich; rhodamine G, National Aniline and Chemical Company; rhodamine 6G, Sigma Chemical Company; erythrosin, Eastman Chemical Company; fluorescein, Sigma Chemical Company. Methylene blue is recrystallized from acetone and allowed to dry in air. Neutral red is recrystallized from methanol and air-dried. All other dyes are used as received. Buffers are prepared using the following reagent grade chemicals: sulfuric acid, potassium chloride, hydrochloric acid, potassium hydrogen phthalate, sodium hydroxide, potassium dihydrogen phosphate, sodium borate, sodium carbonate, and sodium bicarbonate. All buffers are prepared by weight to 0.1 molar concentration. Supporting electrolyte for transfer experiments is reagent grade sodium perchlorate.

All solutions are purged with water-saturated argon purified through vanadous chloride towers for five minutes prior to electrochemical experiments. During the experiments, argon is passed over the top of the solution. All experiments are performed at room temperature and pressure.

A polyelectrolyte, Nafion, is used for one experiment. The Nafion is purchased from CG Processing, Inc. in the form of 5% by weight solution of 1100 equivalent weight in isopropanol. Before use the Nafion solution is diluted to .5% in isopropanol. It is then pipetted onto the electrode surface and the solvent allowed to evaporate in air. The structure of Nafion is shown in figure 8.

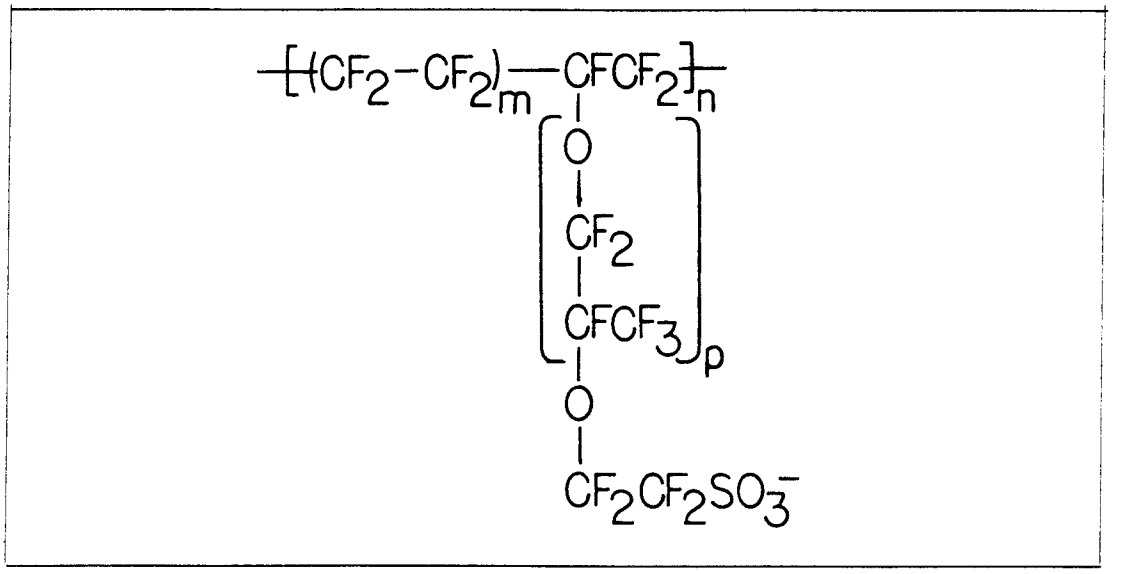

Figure 8: Nafion structure.

2.2 Instrumentation and Methods

All electrochemical experiments are performed in a standard H-cell, with the working and auxiliary electrodes in the same compartment. The saturated sodium chloride calomel reference is in a different compartment separated by a porous glass frit. The auxiliary or counter electrode is a platinum wire cleaned with acetone and deionized water between uses. The working electrodes consist of glassy carbon (0.36 cm^2), edge plane pyrolytic graphite (0.36 cm^2), and basal plane pyrolytic graphite (0.17 cm^2), all from Union Carbide Company. The electrodes are prepared by mounting the graphite onto a glass tube with heat-shrink tubing. The electrical connection consists of a copper wire to a pool of mercury on top of the graphite. Electrode surfaces are prepared as follows. Glassy carbon and edge plane graphite (EPG) surfaces are prepared by wet polishing on silicon carbide sandpaper until the surface looks uniform. This is followed by polishing with one micron alpha alumina until the surface has a very

shiny appearance. The electrode is then rinsed with deionized water, sonicated for a few seconds and rinsed with water again. The surface is then wiped with an acetone-soaked tissue and rinsed with acetone. Basal plane graphite (BPG) electrode surfaces are prepared by cleaving the surface with a clean razor blade. The surface is then treated with acetone like the EPG electrodes.

A tin oxide coated electrode was also used. Electronic connection was made by attaching a copper wire to the tin oxide with silver paste and then covering the silver paste with a hard epoxy to avoid oxidation of the silver.

Cyclic voltammetry was performed using the three electrode system. The electrochemistry was done using a Princeton Applied Research model 173 potentiostat with an EG&G Parc model 175 programmer, and a Houston Instrument 2000 XY recorder. Chronocoulometric measurements were done by connecting the recorder to the Princeton Applied Research model 179 digital coulometer. Fast cyclic voltammograms were performed with the same electrochemical apparatus connected to a Tektronix 5223 digitizing oscilloscope output to the Houston recorder. All cyclic voltammograms shown are numbered with respect to first and subsequent scans.

All spectra were taken on a Hewlett-Packard 8450A uv/vis spectrophotometer. pH measurements were made on an Beckman digital pH meter.

Although none of the fluorometric experiments have been performed to date, the laser-induced fluorescence spectrophotometer is of interest to this project. The apparatus and spectroelectrochemical cell are described in appendix 1.

3. RESULTS AND DISCUSSION

3.1 Methylene Blue Study

Methylene blue (3,7-bis-dimethylaminophenothiazinium chloride), figure 9,

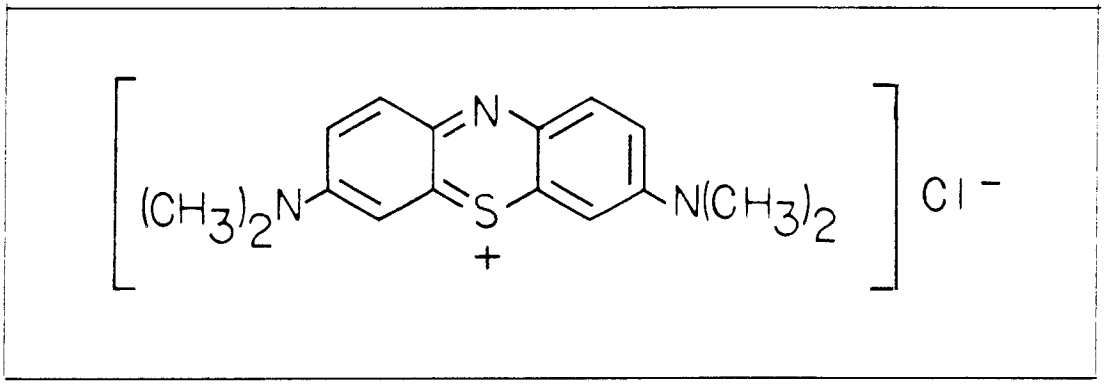

Figure 9: Methylene blue structure.

was chosen as a dye to study adsorption characteristics in detail since its solution chemistry and electrochemistry had been studied previously.[23-27] It proved to adsorb to the electrode surface reproducibly and could be kept on the surface for long periods of time. Both of these considerations are of importance for the luminescence experiments.

3.1.1 pH Dependence of Redox Potentials

Methylene blue undergoes a two electron reduction to leucomethylene blue, shown in figure 10. In solution, the amine nitrogens of methylene blue are very weakly basic and are never protonated. The bridging nitrogen is strongly basic, and is protonated over the pH range 1-13. After reduction to leucomethylene blue, the amine groups can be protonated, with $pK_a(1) = 5.02$ and $pK_a(2) = 5.87$.[25] One factor to notice is that in basic pH, the leucomethylene blue has no charge, and hence becomes sparingly soluble in aqueous solution. The reduction potential is pH dependent as shown later. As

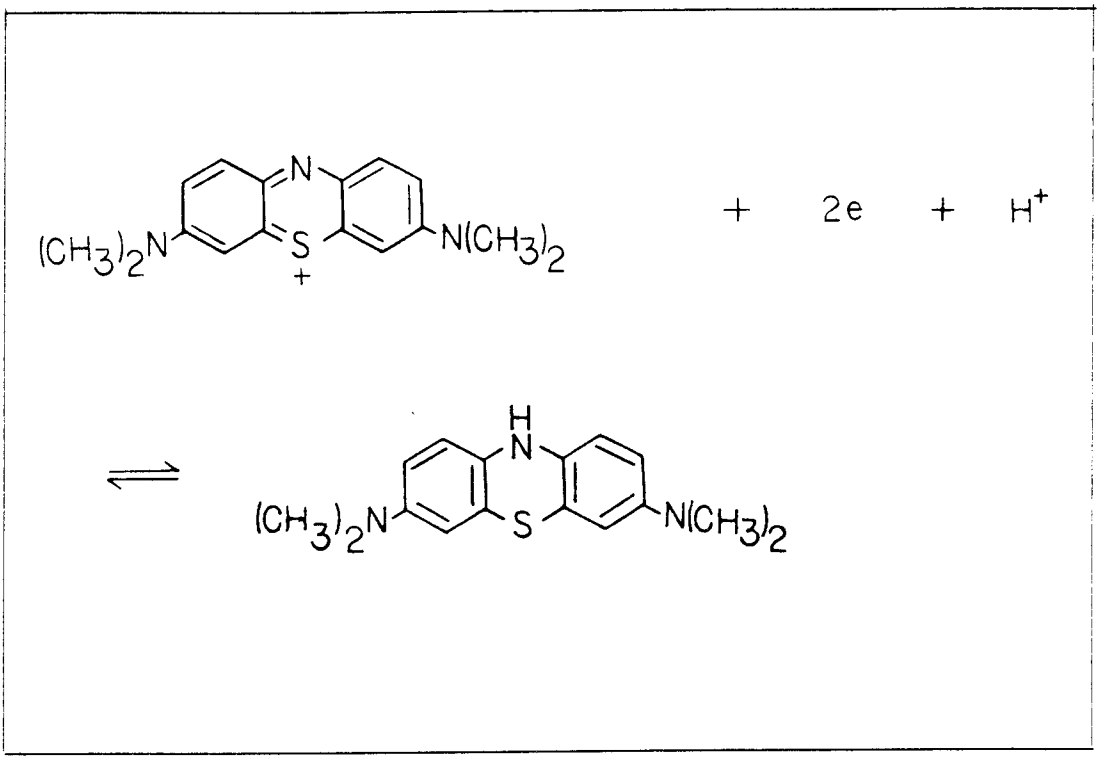

Figure 10: Reduction of methylene blue to leucomethylene blue.

the pH decreases, the amine groups of the reduced species are able to be protonated and the pH effect is increased. By using the Nernst equation, one can predict the slope of a plot of pH vs. formal potential, E_0. The table in figure 11 shows the predicted slope over three pH ranges. Appendix 2 shows the reductions for the variable values of x in the following equation.

$$E = E_0 + \frac{RT}{nF} \ln \frac{[Ox]\,[H^+]^x}{[Red]}$$

Experimental results are in agreement with these predictions. A plot of E_0 vs. pH, figure 12, gives a curve on which three straight lines can be drawn in the three pH ranges with slopes close to the predicted values. These E_0 values are for the methylene blue species adsorbed on EPG. The values closely parallel

pH range	x	Predicted slope
1-5	3	88 mV
5-6	2	59 mV
6-12	1	30 mV

Figure 11: Predicted slopes of E_0 vs. pH plot.

those of Clark's study of methylene blue redox potentials in solution.[23] There is a slight negative shift in reduction potential for the adsorbed methylene blue, corresponding to the stabilization of the complex on the surface.

3.2 Methylene Blue Dimerization

Methylene blue solution spectra are shown in figure 13. The predominant feature of methylene blue solution chemistry is its monomer-dimer equilibrium. The most stable dimer configuration is two monomer units stacked with the principal axis parallel and the bridging nitrogen of one monomer unit opposite the sulfur atom of the second, figure 14.[28] The equilibrium constant, K_{eq}, has been determined to be $3.97 \times 10^3\ M^{-1}$ [24], resulting in the dimer being present at concentrations as low as 10^{-5} M. The table in figure 15 shows the percentage of dimer present at various concentrations of methylene blue. Methylene blue, at higher concentrations, can form trimers and various other oligomers. There is inconclusive evidence that leucomethylene blue ever dimerizes.

The polymerization of dyes is due mainly to Van der Waals forces. London's theory of attractive forces predicts that the mutual potential energy of two identical molecules possessing a single long-wave electronic absorption band, λ_0, is proportional to $f^2 \lambda_0^3$, where f is a measure of excitation probability. Therefore

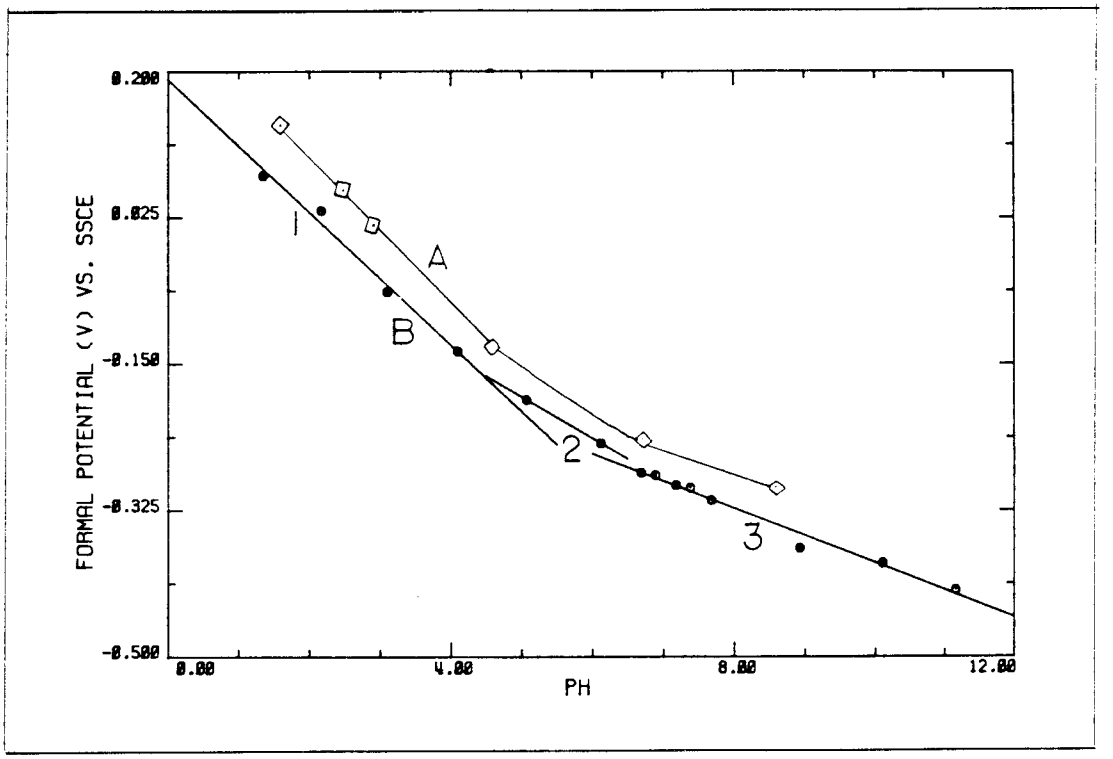

Figure 12: pH dependence of methylene blue redox potential. A) solution [23]; B) adsorbed, 1) slope = 79 mV, 2) slope = 49.5 mV, 3) slope = 32.5 mV.

the large values of f and λ_0, which are exactly the properties that make the dyes highly colored, also contribute to stronger attractive forces between molecules. The colorless leucomethylene blue does not have these properties, and therefore is not expected to dimerize. Addition of ethanol can effectively stop dimerization below concentrations of 2×10^{-3}. Stronger solvent interactions prevent molecules from approaching one another.

A 7 mV negative shift in reduction potential occurs upon dimerization. Most of the electrochemical experiments reported here were performed at concentrations where dimerization did not occur to any great extent. Those experiments done at higher concentrations did not result in any noticeable differences

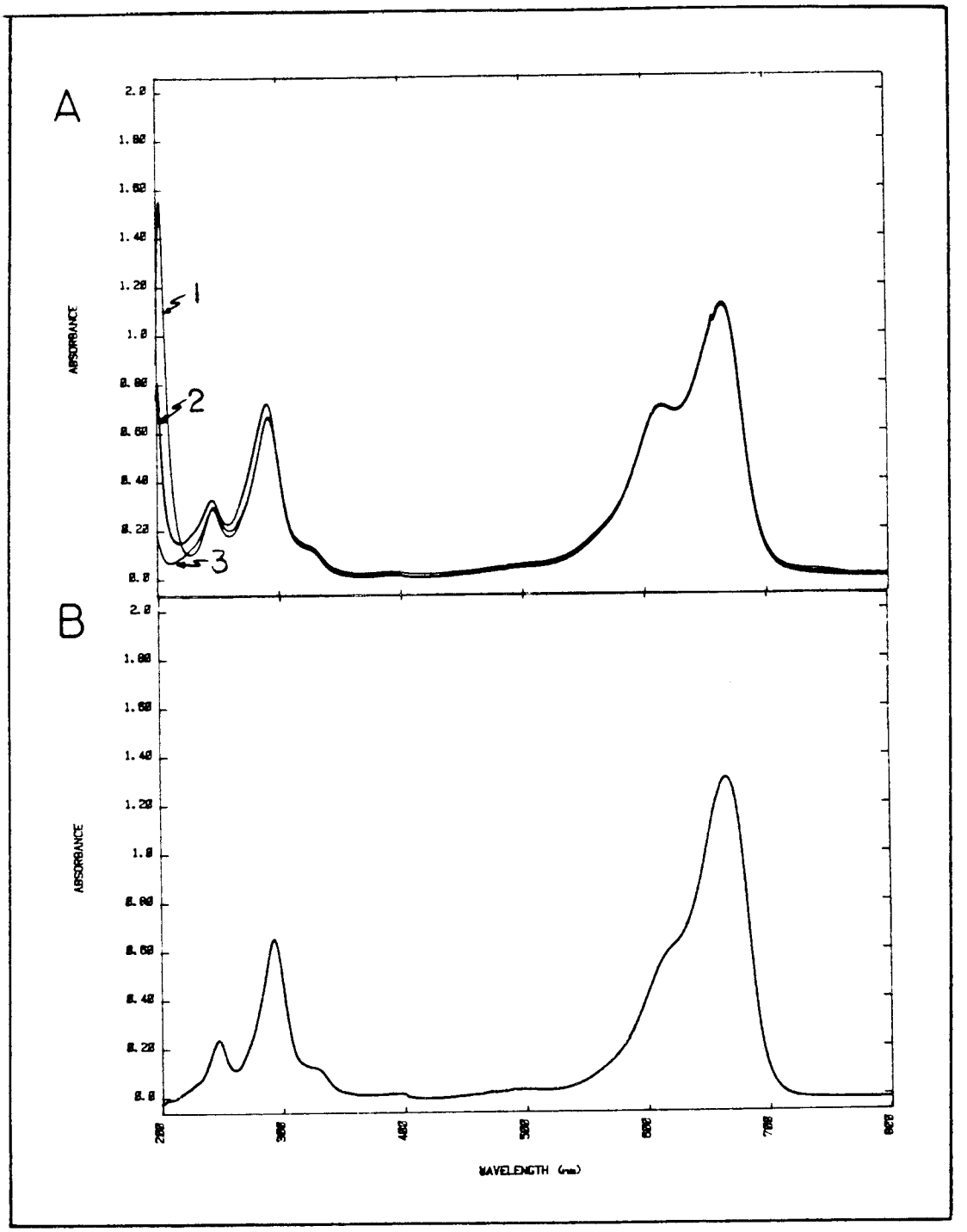

Figure 13: Methylene blue spectra in aqueous and 10% ethanol solutions. 1.5×10^{-5} M methylene blue, path length = 1 cm, ε = 8.9×10^{4} M^{-1} cm^{-1}. Dimer absorption occurs as the shoulder at 610 nm. A) aqueous solution 1) pH = 11.16, 2) pH = 6.93, 3) ph = 1.78; B) 10% ethanol in water.

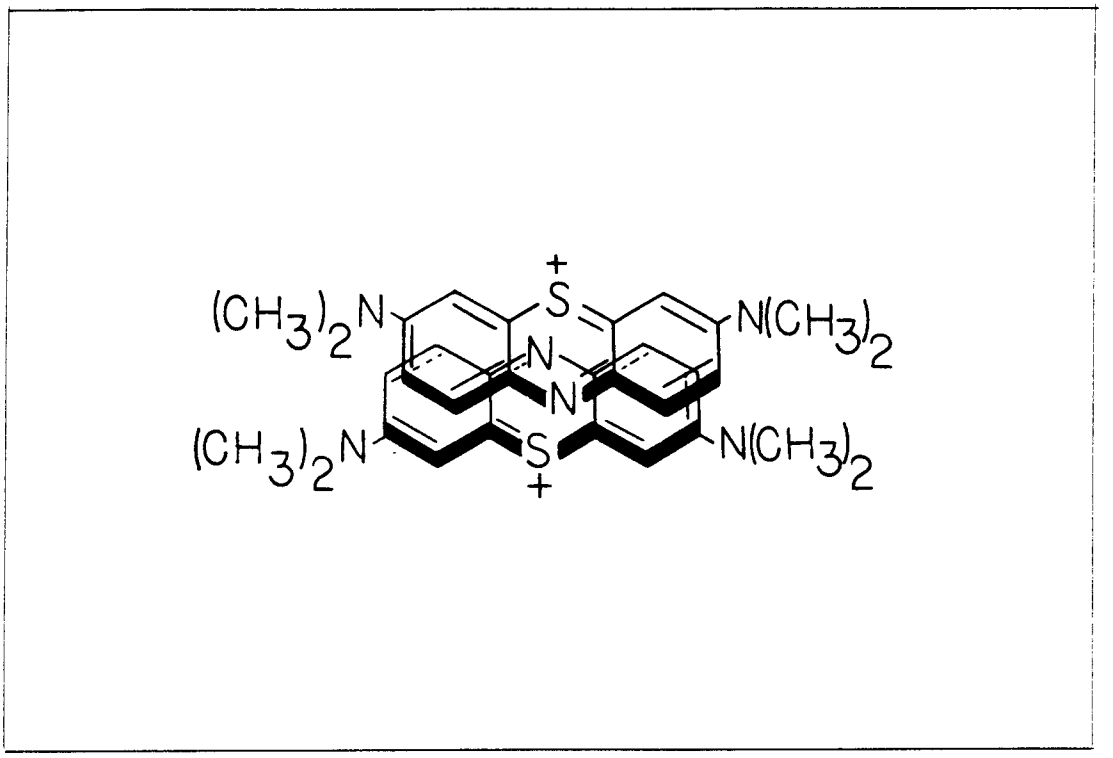

Figure 14: Methylene blue dimer structure.

in adsorption behavior. It is difficult to say in which form methylene blue is adsorbed on the surface. However, it is likely there are interactions between all molecules adsorbed on the surface and, therefore, one could not distinguish adsorbed monomer from adsorbed dimer.

Spectral differences between monomer and dimer can be seen in figure 13. Monomer absorption occurs at λ = 660 nm, while dimer absorption is at λ = 610 nm. At 610 nm, relative extinction coefficients of monomer to dimer are 3.87 x 10^4 M^{-1} cm^{-1}, 9.05 x 10^4 M^{-1} cm^{-1}.[24] The effect of ethanol can also be seen by the disappearance of the dimer peak and shift of the monomer peak.

3.2.1 Surface Electrochemistry

Methylene blue loads quite easily onto electrode surfaces. The electrode is

Methylene blue concentration (M)	% monomer
0	100
2.5×10^{-7}	100
2.5×10^{-6}	99.5
2.5×10^{-5}	95.5
2.5×10^{-4}	73.2
2.5×10^{-3}	35.9

Figure 15: % monomer at various methylene blue concentrations.

immersed in solution and cyclic voltammograms run periodically will show successively substantial increases in peak current, indicating adsorption. The peaks are rather drawn out and asymmetric due to the presence of both solution and adsorbed species. The loading process is complete when there is no further increase in peak current, approximately 45 minutes. Figure 16 shows the increasing adsorption with time.

A transfer of the loaded electrode to a buffered solution containing 0.1 molar $NaClO_4$ gives the following cyclic voltammogram, figure 17. The adsorbed film is quite stable and remains on the electrode surface for periods of 4 hours with less than 10% loss. The $NaClO_4$ is important in limiting the methylene blue-anion solubility. The same transfer experiment, with KCl as a supporting electrolyte will show a 50% or more loss in peak current after only 2 hours. The cyclic voltammograms now appear more symmetrical, with only adsorbed species present.

Since the reduced form of methylene blue is less soluble in water (due to a decreased charge), an effort was made to load the electrode at a potential where

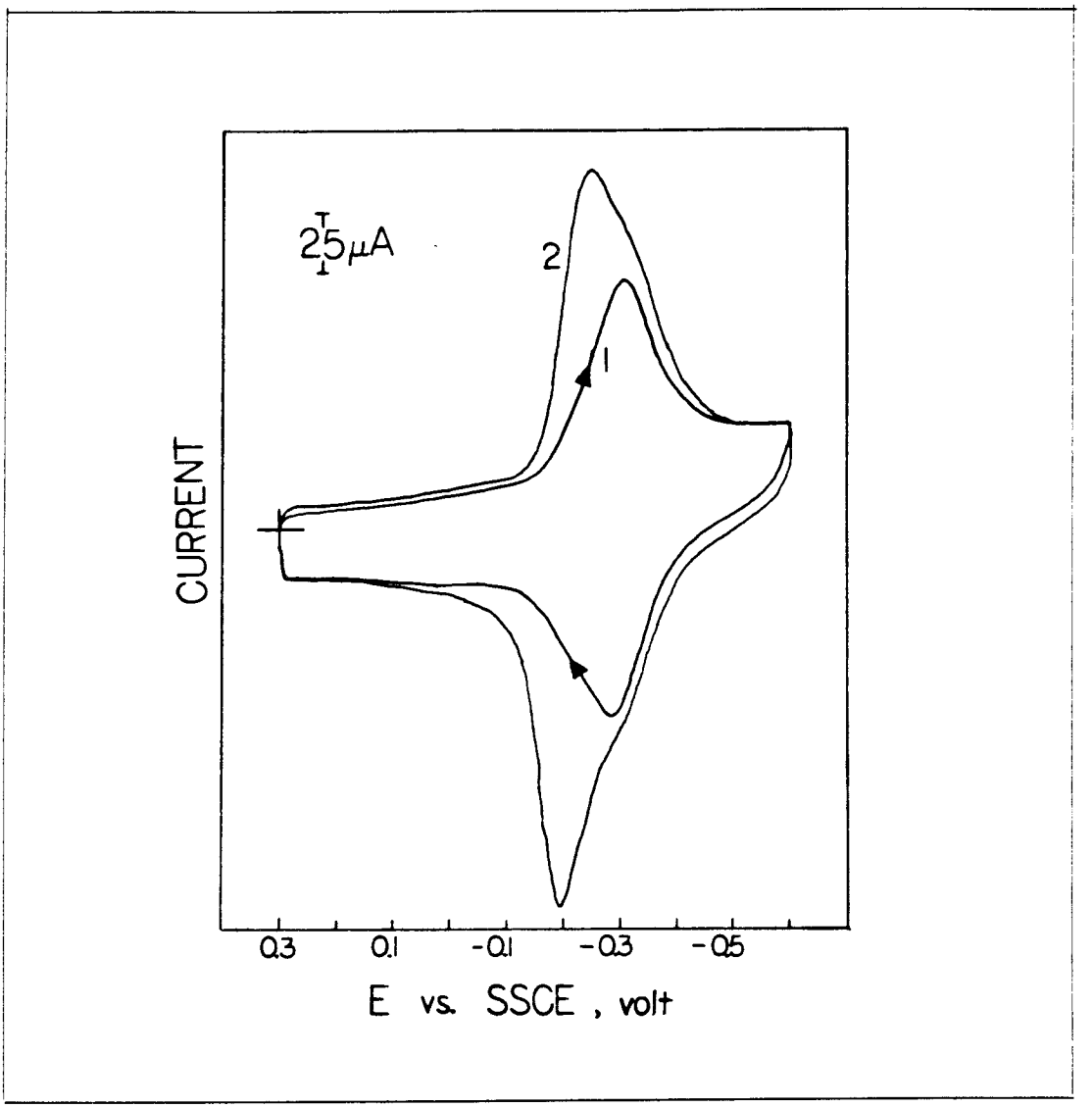

Figure 16: Cyclic voltammograms of methylene blue adsorbing onto the electrode surface from a solution of 0.2 mM methylene blue in 0.1 M phosphate pH 7 buffer.

the methylene blue was reduced to leucomethylene blue. The experiment was done in an oxygen-free environment, since oxygen will reoxidize leucomethylene blue to methylene blue. After the electrode was loaded at -0.6 V and transferred to a 0.1 M $NaClO_4$ supporting electrolyte, the following cyclic voltammogram was obtained, figure 18. The large peak currents obtained

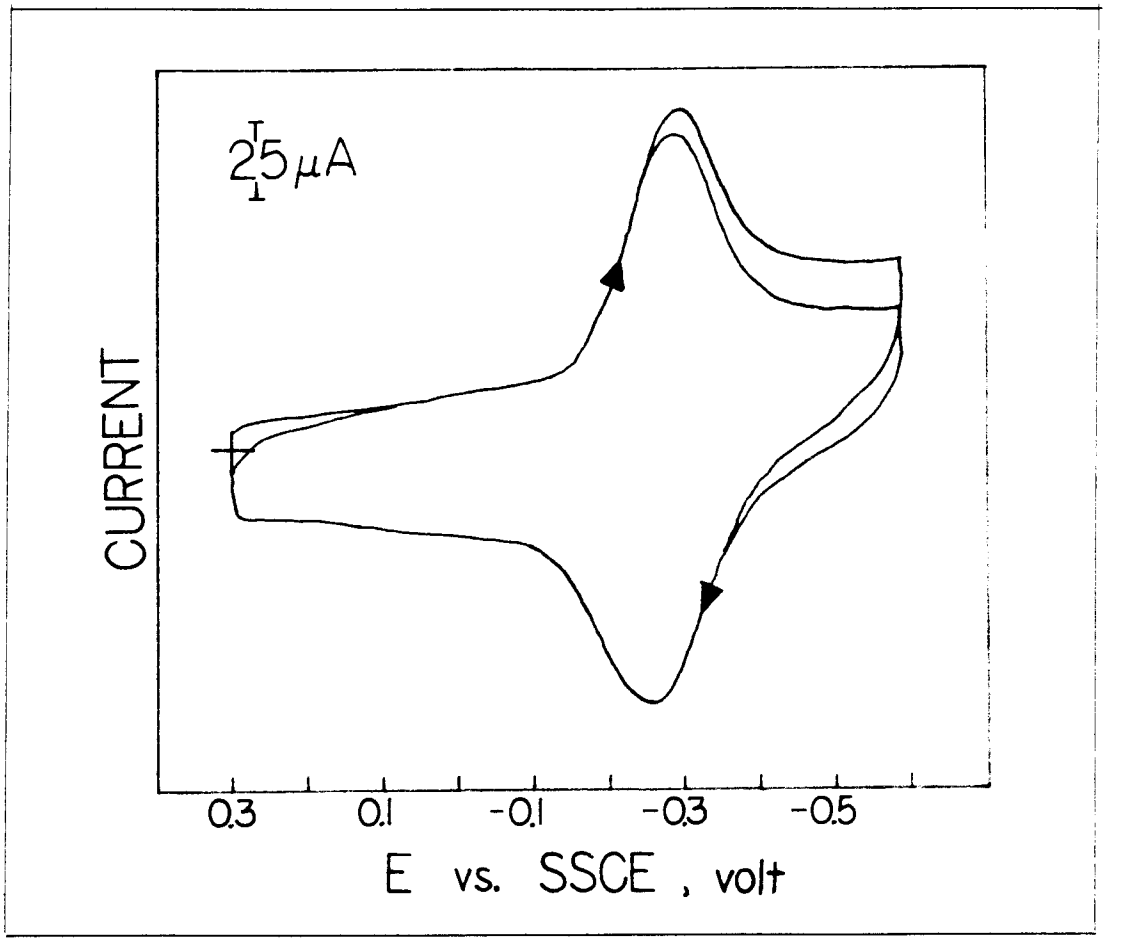

Figure 17: Cyclic voltammogram of methylene blue loaded electrode transferred to 0.1 M $NaClO_4$ supporting electrolyte.

suggest a larger Γ than that obtained by loading in the usual manner. The two peaks seen in the cyclic voltammogram can also be explained by a large amount of adsorption. If the film is thick enough, regions within it may differ enough to separate oxidation and reduction potentials resulting in two waves. Further evidence that the film is very thick could be seen by just looking at the electrode surface. The electrode had a metallic appearance in contrast to electrodes loaded usually on which nothing could be seen. Although much greater surface deposits could be made in this method, the two waves appearing on transfer

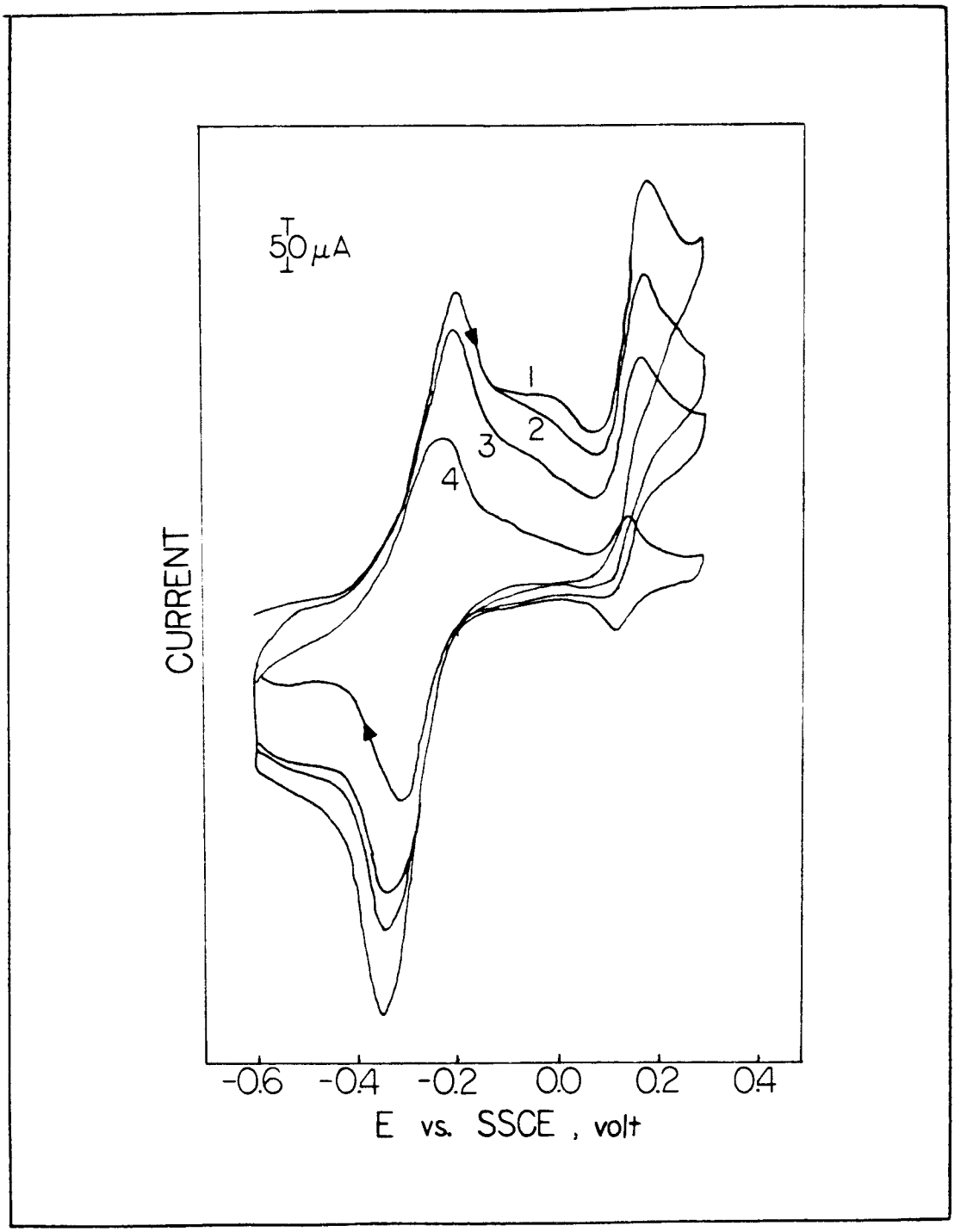

Figure 18: Cyclic voltammogram of methylene blue loaded at -0.6 V in oxygen-free environment and transferred to 0.1 M $NaClO_4$ solution.

make it undesirable for the fluorescence experiments. A simultaneous fluorescence/electrochemical experiment would be difficult to interpret, since not all the material on the surface would be getting oxidized or reduced under the same peak.

The electrochemistry occuring at the electrode surface was then examined in detail. For a surface-bound species, a linear dependence of peak current vs. scan rate is expected for a Nernstian system. The relationship between scan rate and peak current is shown in figure 19. The plot is linear for scan rates up to 1000 mV/sec, after which a negative deviation is seen. This indicates that either IR compensation is not able to correct the uncompensated resistance or that electron-transfer kinetics are becoming nonideal. The phenomenon can also be seen in a plot of the anodic and cathodic peak separation, ΔE_p, vs. scan rate, figure 20. Ideally, for a Nernstian species adsorbed on the electrode surface, the ΔE_p should be 0. In practice, it is difficult to ever see this because of uncompensated resistance. However, for scan rates below 1000 mV/sec, the peak separation is fairly constant, about 35 mV. At faster scan rates, the peak separation increases dramatically.

The surface-bound film was then compared to a thin-layer electrochemical cell, to which the following equation applies.

$$i = \frac{n^2 F^2 v V C^*_o}{RT} \frac{\exp\left[\frac{nF}{RT}\left(E - E_0\right)\right]}{1 + \exp\left[\frac{nF}{RT}\left(E - E_0\right)\right]} = \frac{n^2 F^2 v \Gamma A}{RT} \frac{\exp\left[\frac{nF}{RT}\left(E - E_0\right)\right]}{1 + \exp\left[\frac{nF}{RT}\left(E - E_0\right)\right]}$$

where

i = current;

n = number of electrons;

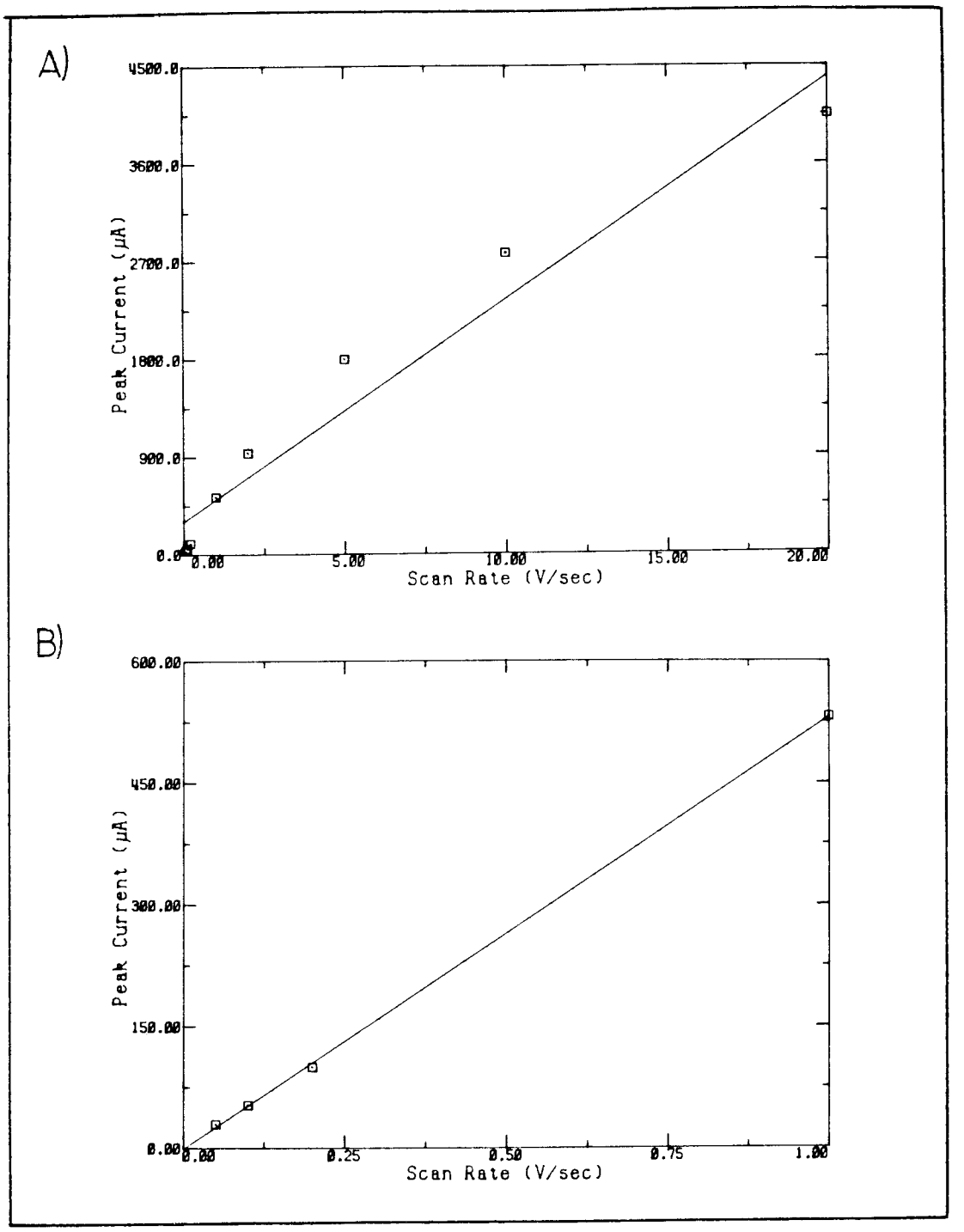

Figure 19: Peak current dependence on scan rate. A) entire range of scan rates; B) linear portion of curve.

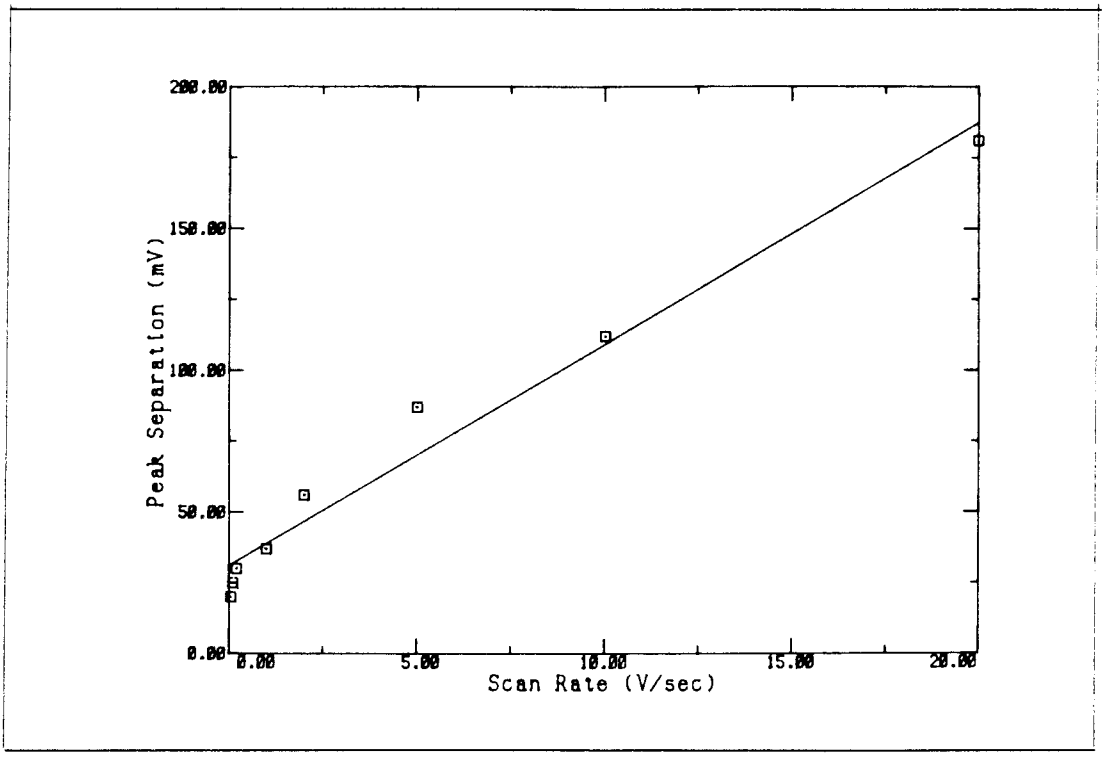

Figure 20: Peak separation dependence on scan rate.

F = Faraday's constant;

v = scan rate;

V = volume of solution in thin layer cell;

C^*_o = bulk concentration;

R = gas constant;

T = temperature;

Γ = surface coverage;

A = area of electrode.

By substituting into this equation the amount of electroactive species found on the surface experimentally, one can calculate a theoretical current-potential curve. This is what the cyclic voltammogram would look like if the adsorbed film was behaving like a true thin layer cell. Figure 21 shows the calculated curve

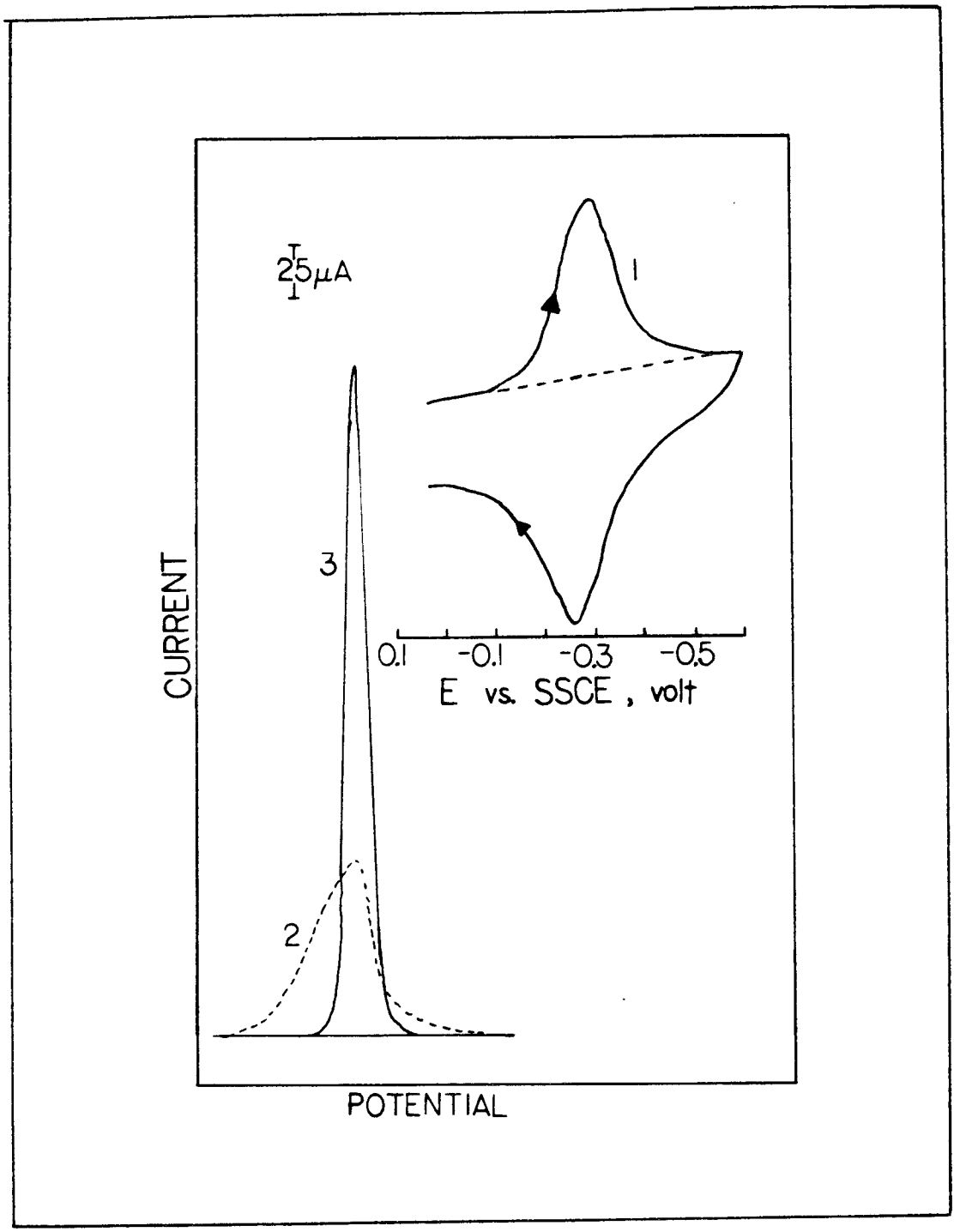

Figure 21: Theoretical current potential curve compared to experimental cyclic voltammogram. 1) experimental cyclic voltammogram; 2) experimental curve; 3) calculated curve for $\Gamma = 12.5 \times 10^{-10}$ moles/ cm^2.

and the experimental cyclic voltammogram. Although the area under the curves is the same, the peak shapes are drastically different. This is due to interactions between the molecules on the surface. The thin layer equation assumes an ideal system in which there are no intramolecular interactions.

3.2.2 Methylene Blue Adsorption

The molecular interaction effect shows up again when one calculates a Nernst plot for the adsorbed methylene blue system. The Nernst equation shown below predicts a slope of 13 mV for a two electron reduction on a plot of $\ln \frac{[Ox]}{[Red]}$ vs. potential. The plot prepared from experimental data gives a slope of 52 mV, figure 22. However, the plot is linear and the intercept, E_0, does not deviate from the expected value. The non-Nernstian slope is due to the strong interaction between molecules in a region of high concentration on the surface.

$$E = E_0 + \frac{RT}{nF} \ln \frac{[Ox]}{[Red]}$$

The amount of methylene blue adsorbed on the surface is determined by a chronocoulometric method in which charge passed, Q, is measured over a time interval. The actual process is recorded in figure 23. The charge is determined by the vertical difference between the two background slopes. Γ, or surface coverage is then calculated by the following equation.

$$\Gamma = \frac{Q}{n F A}$$

where variables are as defined previously. Figure 24 shows isotherms for methylene blue adsorbed on BPG and EPG electrodes. There is increasing surface coverage up to concentrations of 1×10^{-4} M, where the amount of adsorption levels off. On EPG, Γ stops increasing at 12.5×10^{-10} moles/cm^2. By using

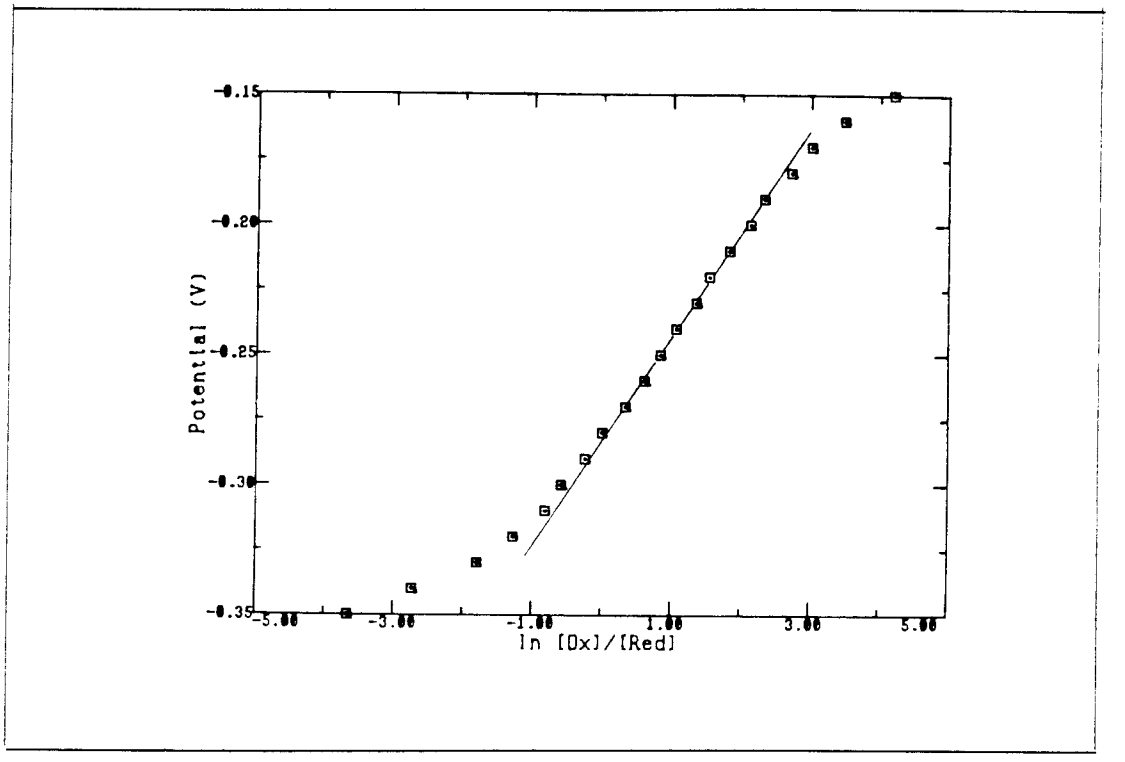

Figure 22: Nernst plot of adsorbed methylene blue reduction.

the molecular dimensions of methylene blue (16 x 8 x 4 Angstroms), possible numbers of adsorbed layers can be calculated.[29]

In any case, the amount adsorbed corresponds to more than one monolayer of methylene blue. In actuality, there is probably a mixture of molecular orientations on the surface, resulting in a surface film consisting of between two and ten layers.

There is slightly more adsorption on EPG surfaces than on BPG. Irreproducible surface coverage is also a problem on BPG. This is due to an inability to get reproducible surface area on BPG. When a new surface is cleaved, one is not likely to get exactly the same area as on the previous trial. Also, unless the

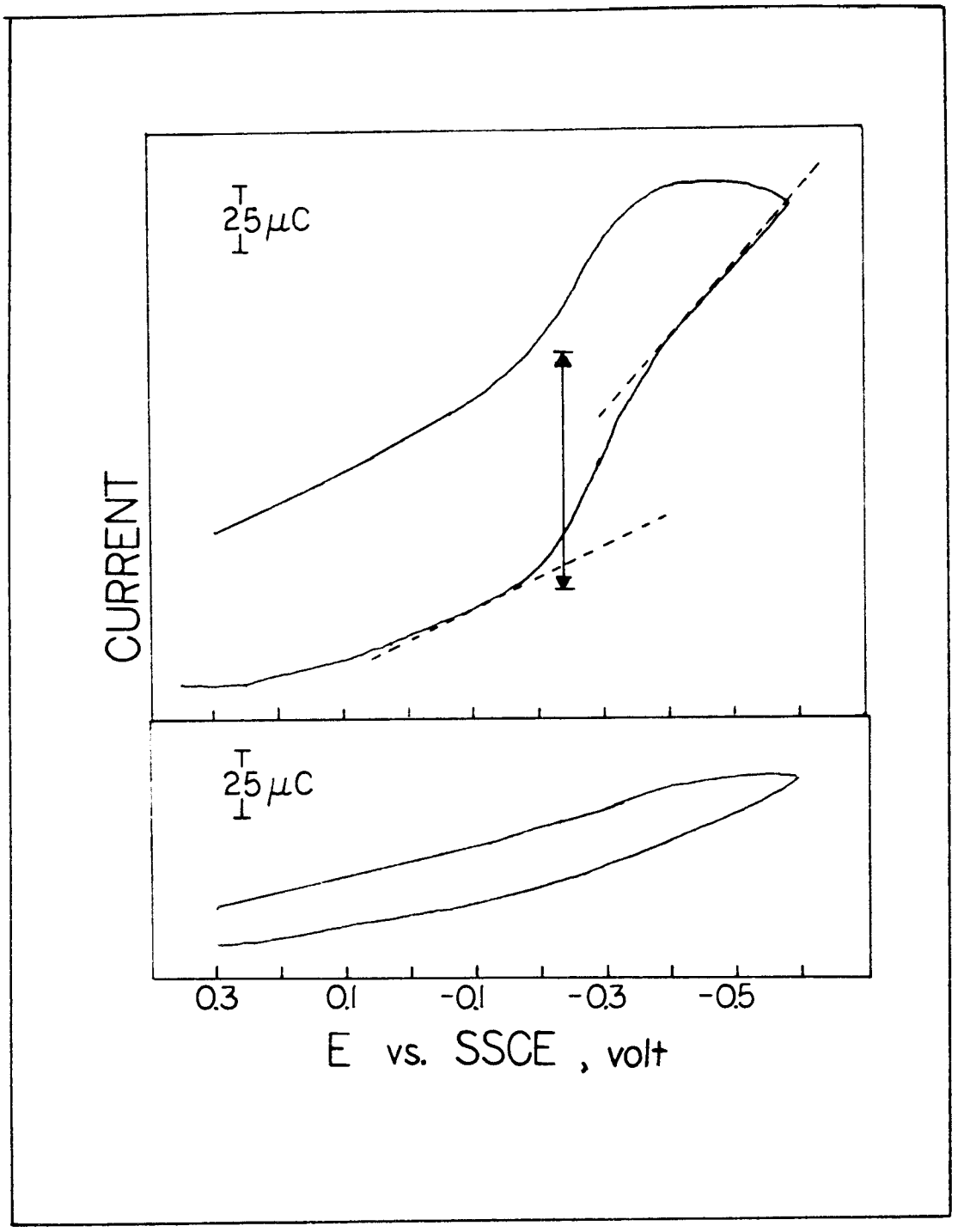

Figure 23: Chronocoulometric recording of methylene blue oxidation and reduction. A) loaded electrode; B) background (0.1 M $NaClO_4$).

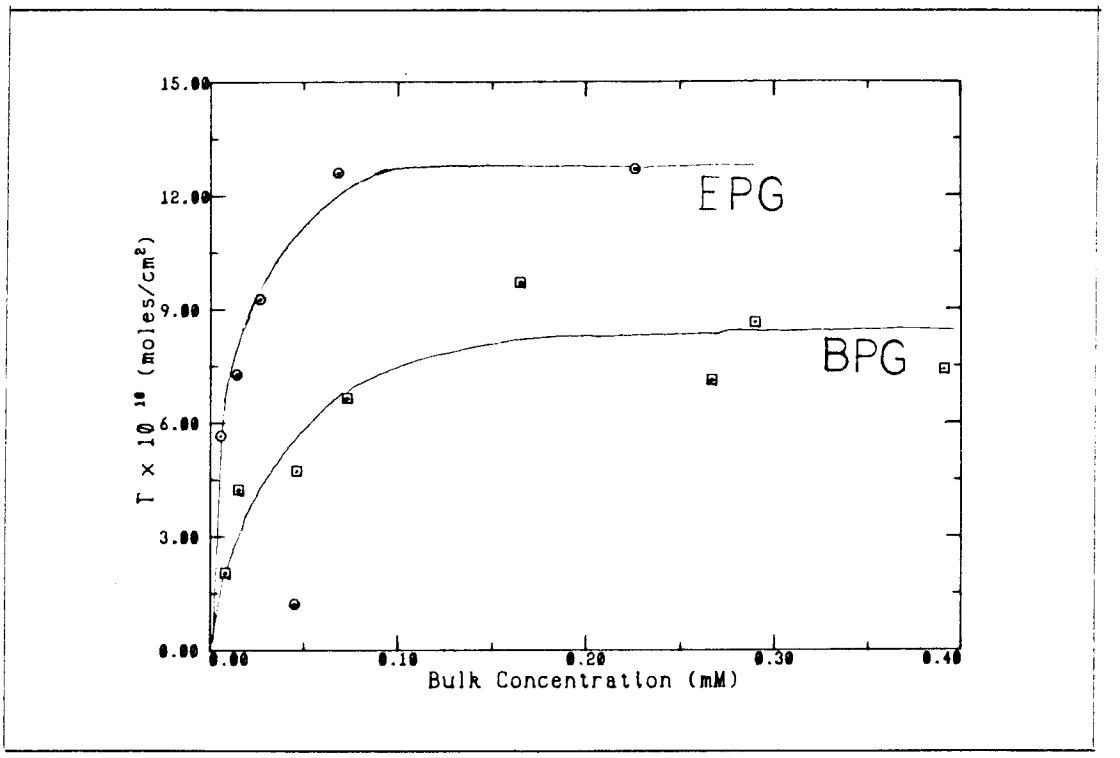

Figure 24: Methylene blue isotherms on BPG and EPG.

cleavage plane is absolutely perfect, the electroactive surface area may differ from the geometrically measured area because of irregular surface features. On the other hand, EPG surfaces prepared by polishing result in more reproducible electroactive areas that are closer to the actual geometric area.

The fact that there is not a vast difference in the amount of adsorption between the two types of graphite is evidence that there is not one preferred molecular orientation. If methylene blue preferred a flat surface orientation, one would expect to see adsorption favored on BPG with the π-cloud of the aromatic rings interacting with the π electrons of the double bonds between the carbon atoms of the graphite. More complex interactions would occur with the broken sp^2 bonds of the EPG carbon atoms.

Molecular orientation	Γ for 1 monolayer	number of layers
flat	1.3×10^{-10}	10
edge	2.6×10^{-10}	4.8
end	5.2×10^{-10}	2.4

Figure 25: Number of layers assuming various molecular orientations for Γ = 12.5×10^{-10} moles/cm^2.

Chronocoulometric experiments only show how much adsorbed electroactive material is present. Additional methylene blue may be adsorbed, but may be electroinactive due to its site on the surface or in the film not favoring electron transfer. This was proven to be false by rinsing a loaded electrode with methanol until a cyclic voltammogram done with that electrode showed only background current. A spectrum of the rinsing was then taken to determine the concentration, from which the total amount of methylene blue present could be calculated. The optically determined amount was 90% of the chronocoulometric Γ. This slight difference is attributed to experimental error or incomplete rinsing since 15 electrodes had to be loaded and rinsed for enough material to be determined optically. Although a complete rinsing was defined when all electroactive material was gone, it is assumed that electroinactive material was removed from the surface also, since it would probably have a weaker interaction than the electroactive molecules.

3.2.3 Nafion Incorporation

An interesting sidetrack was to try to incorporate methylene blue into a polyelectrolyte film, Nafion, on the electrode surface. This would enable one to put a larger amount of methylene blue near the electrode surface. The film was

loaded by soaking the electrode in a 1 mM solution of methylene blue for about 12 hours. At this time the film on the electrode was dark blue. The loaded electrode was then soaked in water for an hour to ensure a more even distribution of species throughout the film. When transferred to a solution of supporting electrolyte, the cyclic voltammogram in figure 26 resulted. The peaks are widely separated, due to slow electron transfer or uncompensated resistance within the film.

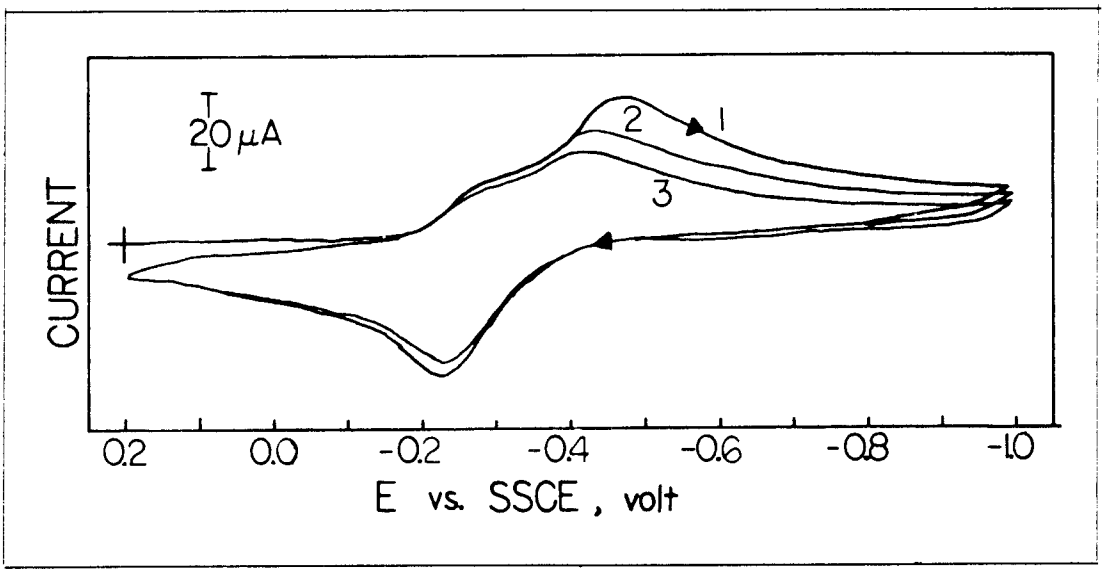

Figure 26: Cyclic voltammogram of methylene blue incorporated in Nafion (2 μl 0.5% Nafion solution pipetted onto electrode).

3.3 Additional Dyes

Other organic dyes were investigated briefly in a study of their adsorption behavior. Their structures are shown in figure 27. Adsorption was attempted on EPG at various pH's and over various potential ranges. The loading processes for some of the dyes under the best conditions are shown in figure 28. The other dyes showed very broad, not well-defined peaks and were not useful to the

project. In fact, only acridine orange showed promise, since it had reversible electrochemistry under the experimental conditions. It also transferred into 0.1 M $NaClO_4$ supporting electrolyte and remained on the electrode surface. Neutral red and Nile blue were quickly lost from the surface, as shown in figure 29.

All of these dyes must be loaded onto the surface by running continuous cyclic voltammograms while in the loading solution. The potential must go out positively enough to oxidize the dye, so some kind of radical mechanism polymerization may occur. A suggested mechanism for molecules with amine hydrogens is shown in figure 30.[30] This is probably what is occuring for the neutral red and Nile Blue species, especially since the shape of their cyclic voltammograms look very similar. Both of these dyes have an amine group and should be able to undergo polymerization at that point.

All of the other dyes could not undergo such a mechanism since their amine groups have non-hydrogen substituents, or they have no amine groups at all. This is reflected in their inability to polymerize onto the electrode surface. Acridine orange is, however, an exception. It is not well understood why acridine orange adsorbs to the surface only when taken out to +1.0 V. An unsuccessful attempt was made to adsorb they species to a tin oxide coated electrode so that a spectrum could be taken of it. However, no indication of adsorption was seen. A spectrum of the material rinsed off the electrode taken by T. Guarr shows little change in band positions from the original solution spectrum. Further experiments may explain the acridine orange behavior.

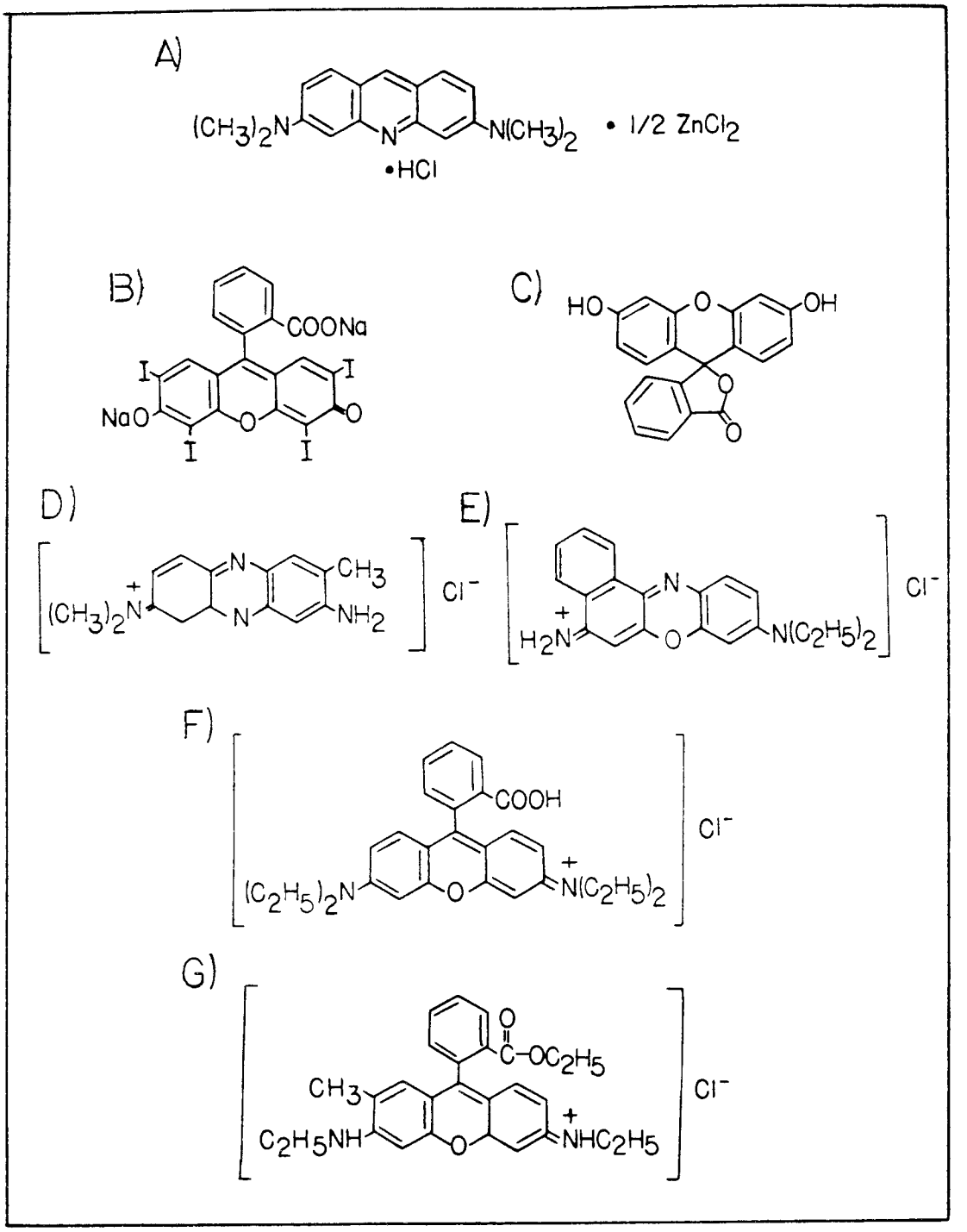

Figure 27: Structure of organic dyes studied. A) acridine orange; B) erythrosin; C) fluorescein; D) neutral red; E) Nile Blue; F) rhodamine B; G) rhodamine 6G.

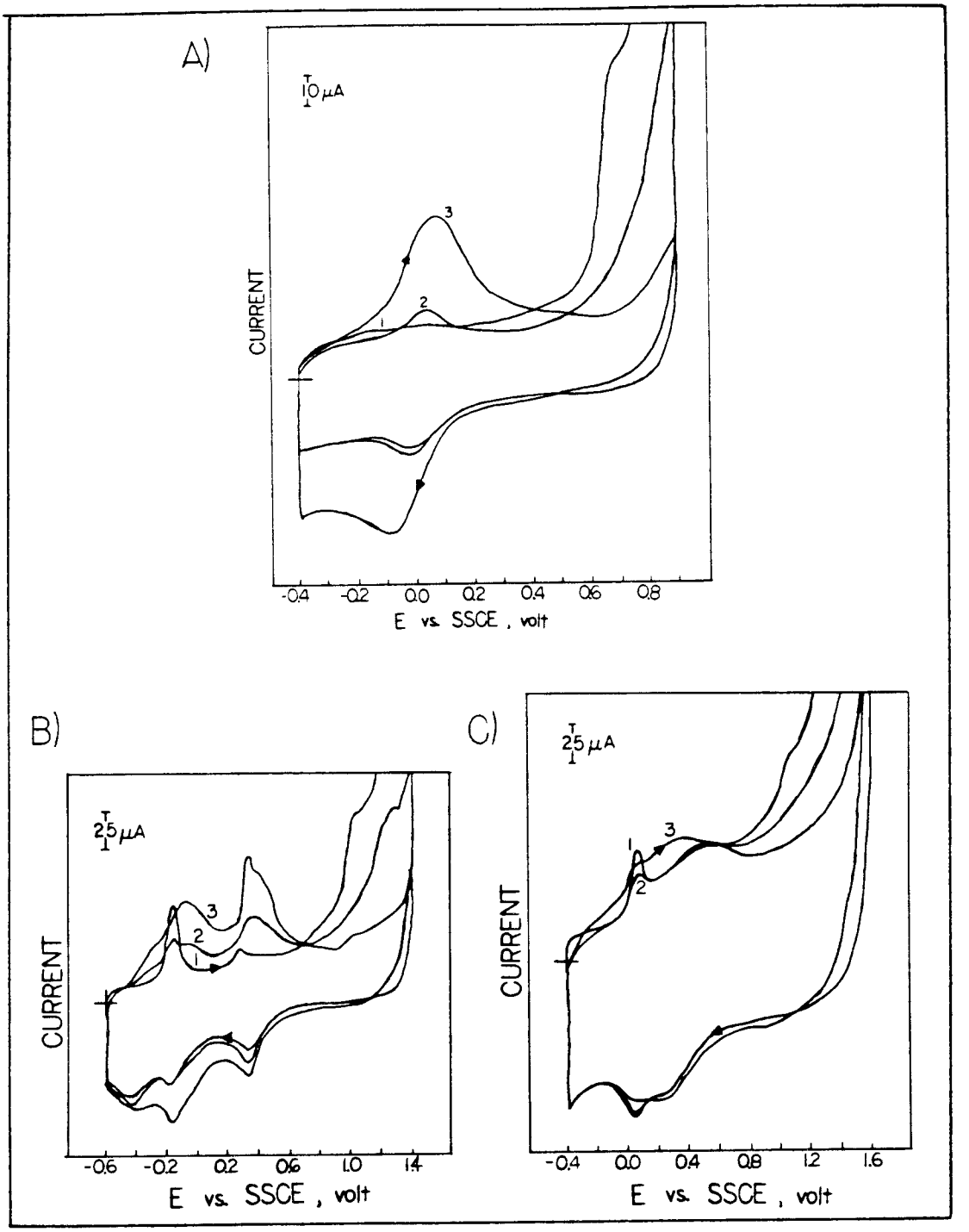

Figure 28: Cyclic voltammograms of dyes adsorbing on electrode surface. A) acridine orange (0.1 M phosphate pH 7 buffer); B) neutral red (0.1 M H_2SO_4); C) Nile Blue (0.1 M H_2SO_4). All dye concentrations are approximately 0.2 mM.

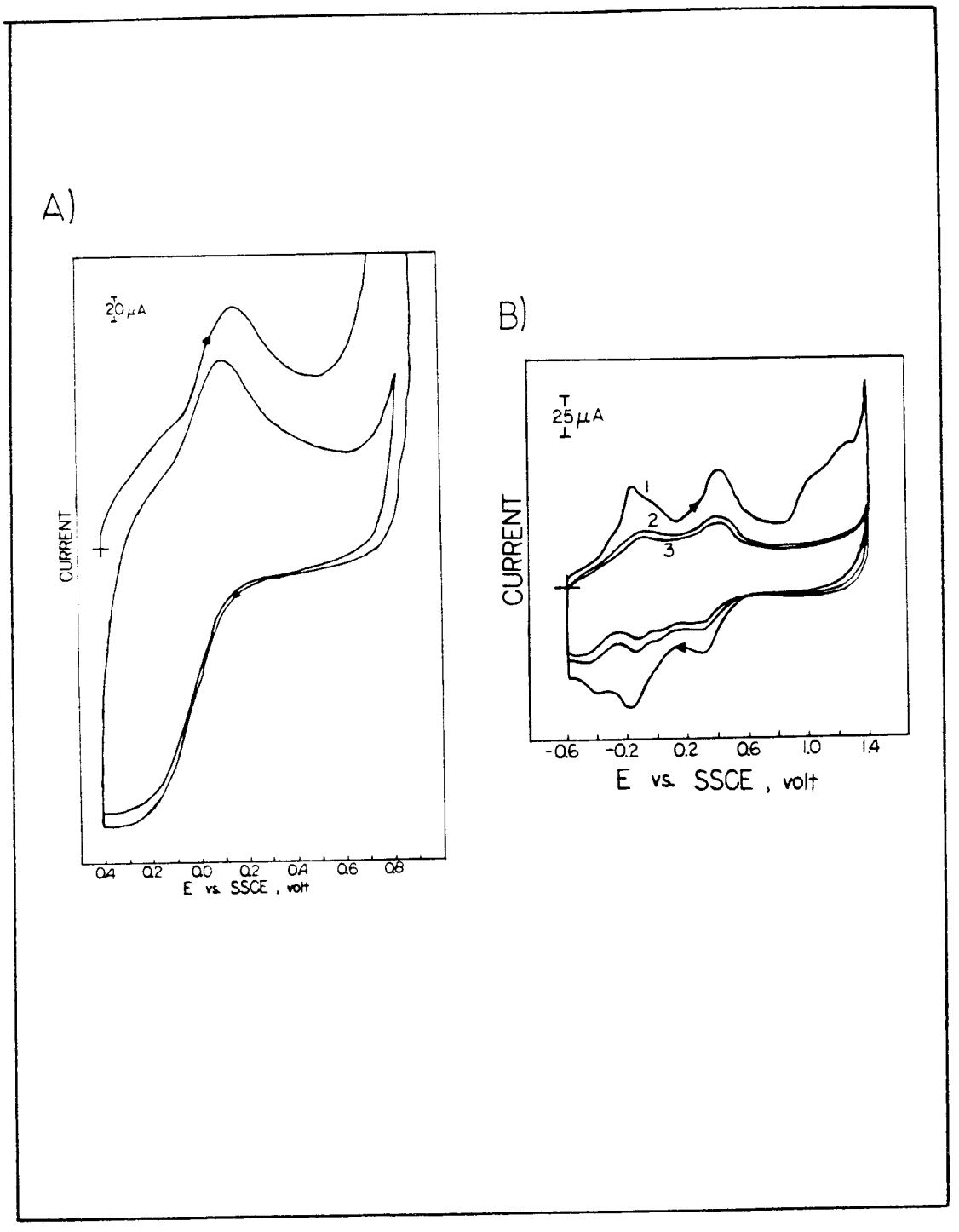

Figure 29: Cyclic voltammograms of loaded electrodes transferred to supporting electrolyte. A) acridine orange (0.1 M phosphate pH 7 buffer); B) neutral red (0.1 M H_2SO_4).

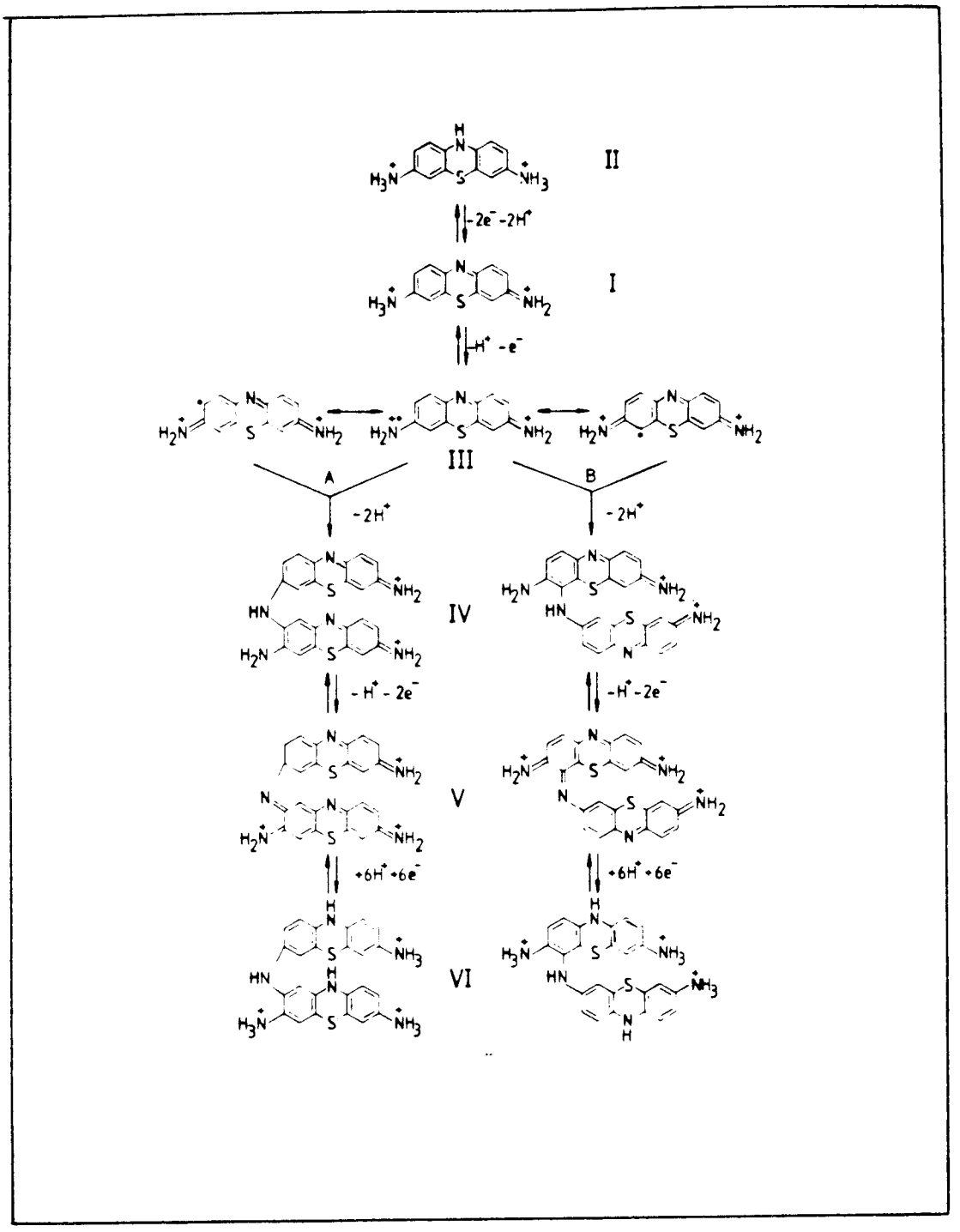

Figure 30: Suggested mechanism for polymerization of thionene.

4. Conclusions

Since the ultimate goal of this project is fluorescence measurements of organic dyes on electrode surfaces, one must examine their fluorescence data. It was impossible to find lifetime or quantum yield data in the literature for some of the dyes, but what could be found is shown in figure 31.

Dye	Solvent	Quantum yield	Lifetime (nsec)	$\lambda_{excitation}$ (nm)
methylene blue	water	0.04	0.4	633
acridine orange[a]	cyclohexane	0.58	9.5	435
rhodamine B[b]	ethanol		3.2	313
rhodamine 6G[b]	water	0.76	3.9	488
fluorescein[b]	0.1 N NaOH	0.9		488

Figure 32: Fluorescence quantum yields and lifetimes of various organic dyes.[31]

It is a disappointment that those dyes with high quantum yields show so little electroactivity and do not appear to adsorb on graphite very well. Acridine orange looks useful since it does adsorb well and has a high quantum yield. However, the lifetimes of these dyes are quite short and would be even shorter on a surface, which may make detection impossible. Nevertheless, the method of electrochemically loading the eyes on the electrode instead of pipetting or dip-coating appears to be worthwhile, since all the material is electroactive.

5. REFERENCES

[1] W.Arden and P.Fromherz, *Ber. Bunsenges. Phys. Chem.*, **82**, 868 (1978).

[2] W.Arden and P.Fromherz, *J. Electrochem. Soc.*, **127**, 370 (1980).

[3] T.Iwasaki, T.Sawada, H.Kamada, A.Fujishma, and K.Honda, *J. Phys. Chem.*, **83**, 2142 (1979).

[4] J.S.Pflug and L.R.Faulkner, *J. Am. Chem. Soc.*, **102**, 6144 (1980).

[5] I.Rubinstein and A.J.Bard, *J. Am. Chem. Soc.*, **103**, 5007 (1981).

[6] D.A.Buttry and F.C.Anson, *J. Am. Chem. Soc.*, **104**, 4824 (1982).

[7] M.Majda and L.R.Faulkner, *J. Electroanal. Chem.*, **137**, 149 (1982).

[8] K.Kemnitz, T.Murao, I.Yamazaki, N.Nakashima, and K.Yoshihara, *Chem. Phys. Lett.*, **101**, 337 (1983).

[9] N.J.Turro, *Modern Molecular Photochemistry*,The Benjamin/Cummings Publishing Co., Inc., Menlo Park, CA, 1978.

[10] D.L.Dexter, *J. Chem. Phys.*, **21**, 836 (1953).

[11] T.Förster, *The Fluorenzenz Organische Verbindungen*, Gottingen: Vandenhoech and Ruprech, 1951.

[12] J.W.Perry, A.J.McQuillan, F.C.Anson, A.H.Zewail, *J. Phys. Chem.*, **87**, 1480 (1983).

[13] N.Mataga and N.Nakashima, *Spectrosc. Lett.*, **8**, 275 (1975).

[14] D.Rehm and A.Weller, *Ber. Bunsenges. Phys. Chem.*, **73**, 834 (1969).

[15] T.J.Meyer, *Acc. Chem. Res.*, **11**, 94 (1978).

[16] C.R.Bock, J.A.Connor, A.R.Gutierrez, T.J.Meyer, D.G.Whitten, B.P.Sullivan, and J.K.Nagle, *J. Amer. Chem. Soc.*, **101**, 4815 (1979).

[17] S.E.Shepard and A.L.Geddes, *J. Am. Chem. Soc.*, **66**, 1995 (1944).

[18] V.L.Ermolaev and A.N.Terenin, *J. Chim. Phys.*, **55**, 698 (1958).

[19] J.Perrin, *Comp. Rend. Acad. Sci. Paris*, **184**, 1097 (1927); **178**, 1978 (1924).

[20] F.Perrin, *Ann. Chem. Phys.*, **17**, 283 (1932).

[21] J.S.Pflug, L.R.Faulkner, and W.R.Seitz, *J. Am. Chem. Soc.*, **105**, 4890 (1983).

[22] K.Itoh, Y.Chiyokawa, M.Nakeo, and K.Honda, *J. Am. Chem. Soc.*, **106**, 1620 (1984).

[23] W.M.Clark, *J. Wash. Acad. Sci.*, **10**, 255 (1920).

[24] W.Spencer and J.R.Sutter, *J. Phys. Chem.*, **83**, 1573 (1979).

[25] R.H.Wopschall and I.Shain, *Anal. Chem.*, **39**, 1527 (1967).

[26] F.Pergola, G.Piccardi, and R.Guidelli, *J. Electroanal. Chem.*, **83**, 33 (1977).

[27] V.Svetlicic, J.Tomaic, and V.Zutic, *J. Electroanal. Chem.*, **146**, 71 (1983).

[28] K.Bergman and C.O'Konski, *J. Phys. Chem.*, **67**, 2169 (1963).

[29] J.W.Galbraith, C.H.Giles, A.G.Halliday, A.S.A.Hassan, D.C.McAllister, N.Macaulay, and N.W.Macmillan, *J. Appl. Chem.*, **8**, 416 (1958).

[30] J.M.Bauldrey and M.D.Archer, *Electrochimica Acta*, **28**, 1515 (1983).

[31] a) V.H.Schäfer, R.Stahn, and W.Schmidt, *Z. Phys. Chem. (Leipzig)*, **260**, 862 (1979); b) I.B.Berlman, *Handbook of Fluorescence Spectra of Aromatic Molecules, 2nd ed.*, Academic Press, New York, 1971.

Appendix 1: Spectroelectrochemical Apparatus

The fluorescence experiments are performed on the apparatus shown in figure 33.

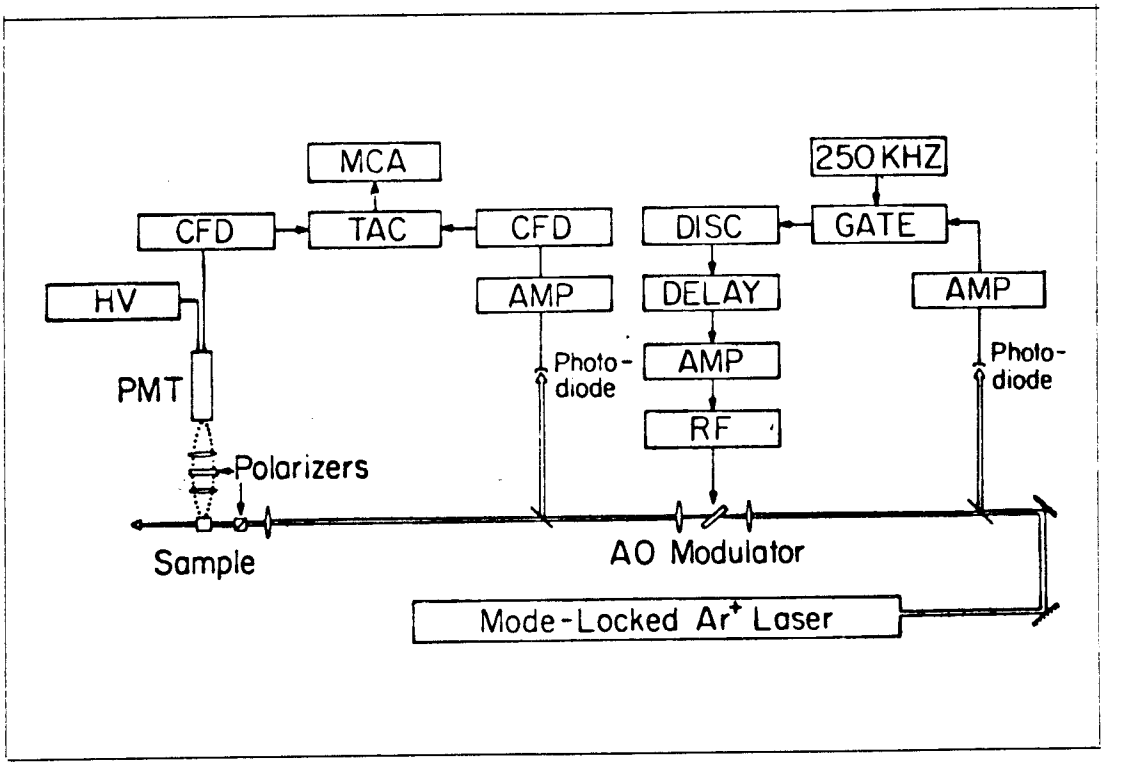

Figure 33: Block diagram of laser-induced fluorescence apparatus.

A Spectra Physics model 171/342 mode-locked argon ion laser produced 100 picosecond pulses at a repetition frequency os 82.190 MHz. At a wavelength of 514.5 nm, the average power output is 900 mW. A Spectra Physics model 365 acousto-optic modulator with model 465 rf driver samples the excitation pulses at a frequency of 250 kHz. The modulator is synchronized to the laser output. This is done by focusing a small percentage of the laser output onto a Hewlett-Packard 5082-4203 fast photodiode. The resulting electrical pulses are gated at the desired frequency (depending on the fluorescence lifetime of the species of

interest) with an ORTEC model LG 101 fast linear gate and model 436 discriminator. The gated pulses then trigger the rf driver via a variable delay.

An ORTEC model 457 time-to-amplitude converter was initiated by a portion of the laser output via a fast photodiode and an ORTEC model 473A constant fraction discriminator. Fluorescence is detected at 90° relative to the incident laser beam. An Amperex XP2020Q photomultiplier is used to detect the fluorescence intensity. It is output to an ORTEC model 583 constant fraction differential discriminator which terminates the time-to- amplitude converter. The time-to-amplitude converter is output to a Tracor-Northern TN-1706 multichannel pulse-height analyzer interfaced to a PDP 11/23 computer for data processing and storage.

The proper excitation wavelenth for the various dyes is obtained through a series of nonlinear optics and frequency doublers.

The electrochemical cell used in conjunction with the fluorescence experiments is shown in figure 34. A standard three electrode cell is used with the electrochemical apparatus described previously.

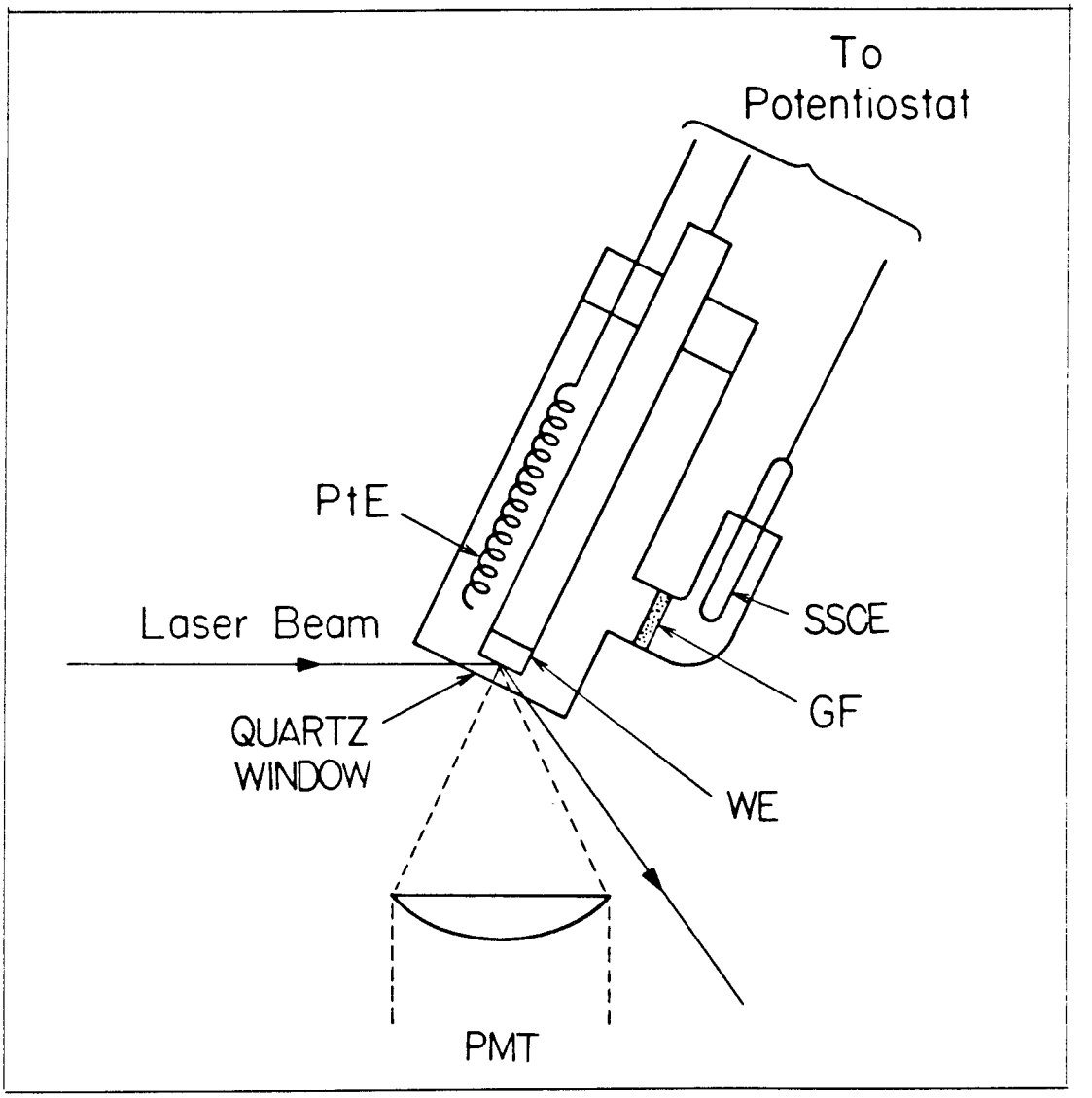

Figure 34: Spectroelectrochemical cell.

Appendix 2: Methylene Blue Reductions

pH = 1 - 5

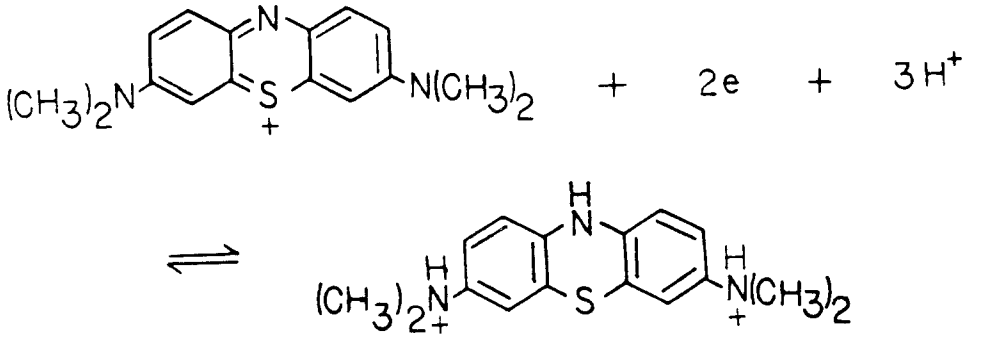

pH = 5 - 6

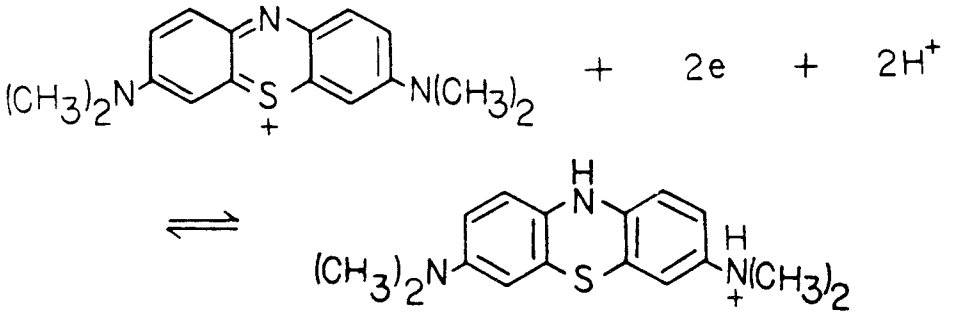

pH = 6 - 13

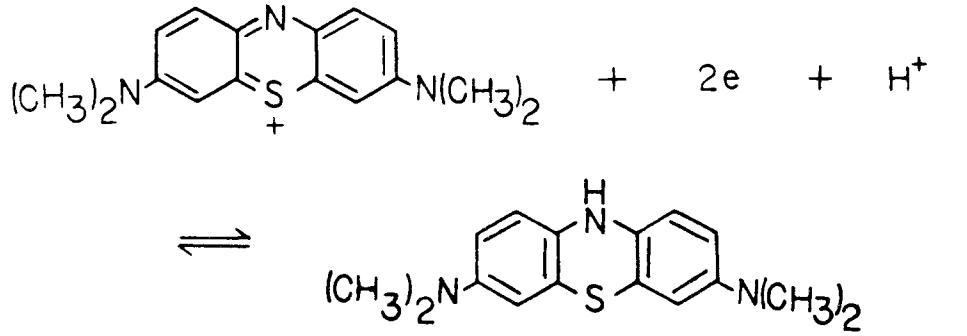

Appendix 3: Data Tables

8.1 Theoretical i-E Curve for a Thin-Layer Cell

E (V)	i_{calc} (amps)
-0.20	1.79×10^{-7}
-0.21	3.89×10^{-7}
-0.22	8.47×10^{-7}
-0.23	1.84×10^{-6}
-0.24	4.00×10^{-6}
-0.25	8.66×10^{-6}
-0.26	1.86×10^{-6}
-0.27	3.92×10^{-5}
-0.28	7.99×10^{-5}
-0.29	1.51×10^{-4}
-0.30	2.51×10^{-4}
-0.31	3.33×10^{-4}
-0.32	3.33×10^{-4}
-0.33	2.51×10^{-4}
-0.34	1.51×10^{-4}
-0.35	7.99×10^{-5}
-0.36	3.92×10^{-5}
-0.37	1.86×10^{-5}
-0.38	8.66×10^{-6}
-0.39	4.00×10^{-6}
-0.40	1.84×10^{-6}
-0.41	8.47×10^{-7}
-0.42	3.89×10^{-7}
-0.43	1.79×10^{-7}

Table of data for theoretical cyclic voltammogram, figure 21.

8.2 Isotherm Data

Bulk Concentration (M)	Γ (moles/cm^2)
2.26×10^{-4}	1.27×10^{-9}
6.81×10^{-5}	1.26×10^{-9}
2.65×10^{-5}	9.27×10^{-10}
1.41×10^{-5}	7.28×10^{-10}
5.50×10^{-6}	5.66×10^{-10}
4.50×10^{-5}	1.22×10^{-9}

Methylene blue isotherm data on EPG, figure 24.

Bulk Concentration (M)	Γ (moles/cm^2)
3.91×10^{-4}	7.41×10^{-10}
2.90×10^{-4}	8.64×10^{-10}
2.67×10^{-4}	7.12×10^{-10}
1.65×10^{-4}	9.70×10^{-10}
7.25×10^{-5}	6.65×10^{-10}
4.58×10^{-5}	4.73×10^{-10}
1.53×10^{-5}	4.24×10^{-10}
7.92×10^{-6}	2.05×10^{-10}

Methylene blue isotherm data on BPG, figure 24.

8.3 Variation of Scan Rate Data

v (V/sec)	i_p (μA)	ΔE_p (mV)
0.05	29.5	20
0.10	53.0	25
0.20	100.0	30
1.00	531.3	37
2.00	937.5	56
5.00	1800	87
10.00	2775	112
20.00	4050	181

Peak current and separation dependence on scan rate, figures 19, 20.

8.4 Nernst Plot Data

E (V)	ln [Ox]/[Red]
-0.15	4.20
-0.16	3.49
-0.17	3.01
-0.18	2.72
-0.19	2.33
-0.20	2.13
-0.21	1.83
-0.22	1.54
-0.23	1.35
-0.24	1.06
-0.25	0.84
-0.26	0.61
-0.27	0.34
-0.28	0.01
-0.29	-0.24
-0.30	-0.58
-0.31	-0.81
-0.32	-1.27
-0.33	-1.79
-0.34	-2.73
-0.35	-3.66

Nernst plot data, figure 22.